Electrical Engineering Theses

Electrical Engineering

Spring 5-23-2014

Midrange Magnetically-Coupled Resonant Circuit Wireless Power Transfer

Varun Nagoorkar

Follow this and additional works at: https://scholarworks.uttyler.edu/ee_grad

Part of the Electrical and Computer Engineering Commons

MIDRANGE MAGNETICALLY-COUPLED RESONANT CIRCUIT

WIRELESS POWER TRANSFER

by

VARUN NAGOORKAR

A thesis submitted in partial fulfillment
of the requirements for the degree of
Master of Science in Electrical Engineering
Department of Electrical Engineering

David M. Beams, Ph.D, PE, Committee Chair
College of Engineering and Computer Science

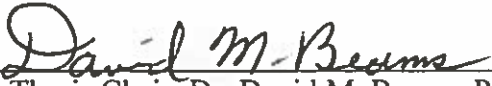The University of Texas at Tyler
May 2014

The University of Texas at Tyler
Tyler, Texas

This is to certify that the Master's thesis of

VARUN NAGOORKAR

has been approved for the thesis requirements on
April 11th, 2014
for the Master of Science in Electrical Engineering

Approvals:

Thesis Chair: Dr. David M. Beams, Ph.D., P.E.

Member: Dr. Hassan El-Kishky, Ph.D., P.E.

Member: Dr. Ron J. Pieper, Ph.D., P.E.

Chair and Graduate Coordinator: Dr. Hassan El-Kishky, Ph.D., P.E.

Dr. James K. Nelson, Jr., Ph.D., P.E.,
Dean, College of Engineering and Computer Science

Acknowledgements

Table of Contents

List of Tables

List of Figures

Abstract

MIDRANGE MAGNETICALLY-COUPLED RESONANT CIRCUIT
WIRELESS POWER TRANSFER

Varun Nagoorkar

Thesis Chair: David M. Beams, Ph. D, PE.

The University of Texas at Tyler

May 2014

Recent years have seen numerous efforts to make wireless power transfer (WPT) feasible for application in diverse fields, from low-power domestic applications and medical applications to high-power industrial applications and electrical vehicles (EVs). As a result, it has been found that WPT by means of non-radiative magnetically-coupled resonant circuits is an optimum method for mid-range applications where the separation of source and receiver is in the range of 1-2m.

This thesis investigates various aspects of the design of magnetically-coupled resonant circuits for non-radiative WPT. Firstly, a basic four-coil network for a mid-range (1-2m gap) WPT system with a single power source and single resistive load was developed and simulated. The system was then constructed and experimental results were obtained for comparison with theoretical expectations. Methodologies were developed for empirical measurement of flux-coupling coefficients (k) among the coupled resonator coils and measurement of resonator parameters (inductance, capacitance, and equivalent-series resistance). Secondly, a structure called a universal resonator is proposed to permit design of WPT networks of arbitrary complexity with multiple power sources (transmitters) and multiple loads (receivers). An Excel simulation tool has been developed to analyze designs involving up to eight resonators. Designs with five resonators (including one power source and two loads) and six resonators (with two power sources and two loads)

with separation of 1m between transmitting and receiving resonators have been analyzed, constructed, and subjected to experimental validation. The measured outputs numerical were found to be in good agreement with the predicted models. Conclusions and suggestions for future work are provided.

Chapter One
Introduction

Wireless power transfer (WPT) is a technique for transferring electrical power from source (transmitter) to load (receiver) without intervening conductors. WPT is a technology which holds the potential to change the way people lead their lives by offering new levels of convenience, mobility and safety. In general there are two types of WPT: (i) near-field (non-radiative coupling) and (ii) far field (radiative coupling). The advantage of near-field non-radiative coupling is that most of the energy that is not being absorbed by the receiver will remain near the source rather than being radiated to surroundings and thus increase the losses in the system. The non-radiative coupling technique is the principal method employed in short- and mid-range (1-2m) WPT systems.

Recent developments have shown a renewed interest in commercial development of WPT using magnetically-coupled resonant circuits (MCRC) for short- and medium-range WPT (distances between source and load are typically1-2m). In this technique, power is transferred between mutually-coupled coils that are tuned to a specific resonant frequency since the most efficient energy exchange will take place among resonators at their resonant frequency. Various applications have been developed based on the MCRC technique, such as wireless charging for battery-operated consumer electronics; medical devices; home appliances; industrial-level high-power applications; and automotive applications. These will be discussed in the next chapter.

In this thesis, magnetically-coupled WPT systems are investigated. Initial investigations concern a WPT system with a single power source and receiver. Subsequently, a universal resonator block for multiple-resonator WPT systems with multiple transmitters and/or receivers has been proposed, and a method for analysis of such systems has been devised. Experimental measurements for validation of the models

have been carried on three systems: a single-source, single-load system; a single-source system with two loads; and a two-source two-load system.

1.1 Organization of Thesis

This thesis is divided into five chapters. Chapter Two discusses development and prior research in WPT beginning with the work of Tesla. Chapter Three describes the basic-four coil network with a single source and load, including a numerical model of the four-coil WPT system and methodologies for determination of resonator electrical parameters and flux-coupling coefficients between resonators. Experimental validation of the model is presented as well. Chapter Four describes a proposed universal resonator block, analytical expressions for WPT with an arbitrary number of resonators, a design tool to analyze WPT systems with up to eight resonators, and numerical models of WPT systems with five resonators (including two loads) and six resonators (including two transmitters and two loads). Chapter Four also includes experimental validation of the numerical models. Chapter Five discusses conclusions and directions for future work.

Chapter Two
Background

2. 1 Tesla's experiments in wireless power transfer

Recent years have seen the introduction by a number of vendors of commercial applications of wireless power transfer (WPT). These applications span a range of power levels and applications; a common application is recharging the batteries of portable devices. Despite this recent activity, the origin of WPT took place a century ago. Nikola Tesla was first to demonstrate the idea of wireless power transfer at the beginning of 20th century with his well-known electro-dynamic induction theory. Efficient mid-range wireless power transfer is possible using resonant circuits, a technique demonstrated by Tesla more than a century ago with the Tesla Coil which produces high-voltage, low-current output with a high-frequency alternating input current. The Tesla coil is a resonant electrical transformer invented about 1891 [1]. Unlike conventional transformer (which has tight flux coupling and a small distance between windings), the Tesla coil consists of loosely-coupled primary and secondary windings separated by a relatively large air gap. Figure (Fig. 2.1) shows a schematic representation of one of the wireless power transfer experiments by Tesla.
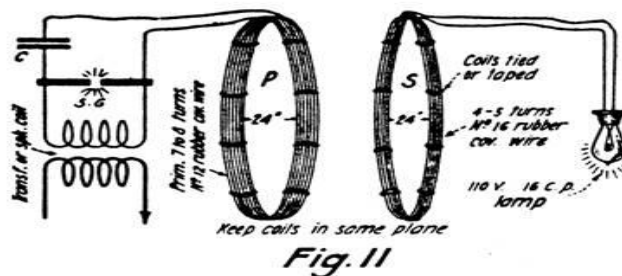
Fig. 2.1 A diagram of one of Tesla's wireless power experiments [2]

In one of his experiments with high frequency (HF) currents, Tesla presented a two coils coupled magnetically and operating under resonance will provide most of its energy at primary (P) to secondary (S). From above Fig. 2.1 one can see that primary (P) is connected to transformer or condenser and spark gap (S.G), when spark breaks the gap primary will get the supply and will light up the 110v, 16 cp (16 candle power or 40W, [2]) lamp connected to secondary (S) even when coils are separated. Tesla also stated that distance of separation can be varied depending upon size and spark coil used for excitation. Tesla presented this phenomenon and provided further description on it in one of lectures in Institution of Electrical Engineers (IEE) at London in 1892 [3]. Later it was proved that these high frequency currents could be used in medical applications as these high frequency currents are harmless and can be passed through body of person without causing any pain or discomfort (below the significantly high limit of current to burn out tissues) [4].

Fig. 2.2 shows a drawing from the patent for wireless energy transmission [5] which was granted to Tesla in 1900, in this figure, the system is seen to consist of a transmitting side and receiving side. In transmitting side of the system, coils C and A form a transformer. Winding A is the secondary of transformer it has many turns and is a large diameter spiral structure. Primary is C has a much shorter length and larger cross-section conductor. Coil C is wound around A and is connected to a source of current G which can be a generator. One terminal of the secondary A is at the center of the spiral coil, and from this terminal the current is led by a conductor B to a terminal D to transmit power to the receiving unit. The other terminal of the secondary A is connected to ground. At the receiving station a transformer of similar construction was employed, with coil A' as the primary winding and coil C' as the secondary winding of the transformer. Elevated terminal D' was used to receive power; it was connected to center of primary coil A' while the other end of A' is connected to ground. Loads (L and M in Fig 1.2) can be connected to secondary coil C'.
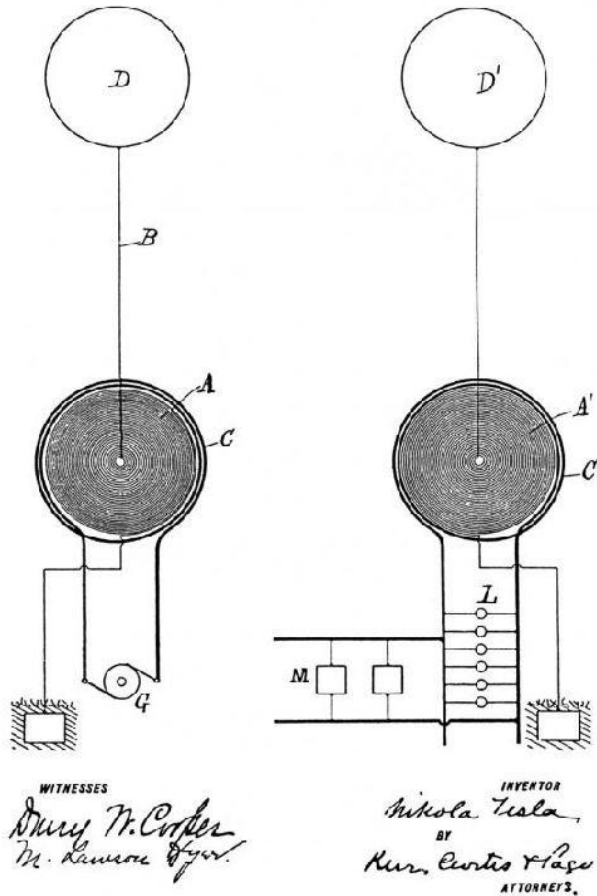
Fig. 2.2 Tesla's wireless energy transmission patent [5]

After demonstrating the principle of WPT at a technical discussion in 1892, Tesla focused his vision on development of a prototype. Tesla constructed a research facility, known as the "Wardenclyffe" tower, where he demonstrated a proof of concept for WPT by transmitting electrical power from the tower to loads without the use of wires. Fig. 2.3 below shows the 187-ft (57.0m) tower. The transmitter was configured to minimize the radiated power, unlike a conventional radio transmitter. Tesla's transmitter's energy was concentrated near surface of ground [6]. The giant transmitter was resonant at 150 kHz and was fed by 300kW of low-frequency power [7, 8]. There are no clear records which describe efficiency and power delivered using this tower; however, Tesla demonstrated the system's performance by lighting 200 incandescent lamps simultaneously while the

transmitting and receiving sides of the system were separated by a distance of 26 miles (42km).

Fig. 2.3 Wardenclyffe tower located in Shoreham, New York [9]

Since the late 1950s wireless power has been an active topic of research. In 1959, a wireless monitoring system using radio pills was developed to study internal conditions of the human body [10-11]. In 1962, an echo capsule (swallowable radio transmitter) was developed for similar purposes; it is energized from outside the human body to transmit information on temperature, acidity or other condition within the digestive tract [12]. Early in the 21st Century, numerous experiments were performed to develop new applications for WPT. In 2007 researchers at MIT (Massachusetts Institute of Technology) used a similar method of resonance to light a fluorescent lamp at a separation of greater than 2m between transmitting antenna and receiving antenna with an output power of 60W at an efficiency of 40% [13].

2. 2 Developments in wireless power transfer (WPT)

Use of power cords is diminishing with the rise of wireless charging systems that are capable of charging portable devices. Though the principles of WPT have been

known for over a century, recent advances have allowed it to be practical. Today WPT is being used in various fields such as consumer electronics, medical devices, the automobile industry, domestic applications, and defense systems.

2.2.1 Development by MIT and Witricity

In 2007, Soljacic and colleagues at MIT demonstrated the feasibility of efficient non-radiative WPT using two resonant loop (self-resonator) antennas. Since then there has been much interest in closely studying the phenomenon. It was found that when two antennas are closely spaced, they are in a coupled-mode resonance region, and in this mode very high power transfer efficiency (PTE) can be achieved [13]. The MIT research team found magnetic resonance as a promising means to transfer power without use of wires because magnetic fields travel freely through air and yet have little effect on the environment and biological systems.

In 2007, the MIT group demonstrated the ability to power a 60W light bulb without use of wires based on strong electromagnetic coupling between resonant objects using non-radiative coupling. Their design consisted of 4 coils; one was used to couple power into the system, two coils served as high-Q LC resonators, and the fourth coil was a load coil connected to a 60W incandescent lamp. The two self-resonant coils were designed to resonate together at 9.9MHz and were separated by 2m with co-axial and coplanar orientations. This apparatus powered the lamp with efficiency of about 40% [13]. Similar results were obtained when the path between the resonators was blocked with a wooden panel. The same apparatus was able to power a 60W bulb with an efficiency of about 90% for separation of 1m between the resonant coils.

After successful demonstrations of mid-range wireless power (on the order of a couple of meters), the MIT group launched a firm named "Witricity" to develop commercial WPT devices using resonant energy transfer in the mW range to kW range. They are developing wireless power applications in fields as diverse as home appliances, mobile devices, automotive applications, and medical devices. Fig. 2.4 below shows typical arrangement of coils in design of MIT for mid-range WPT.
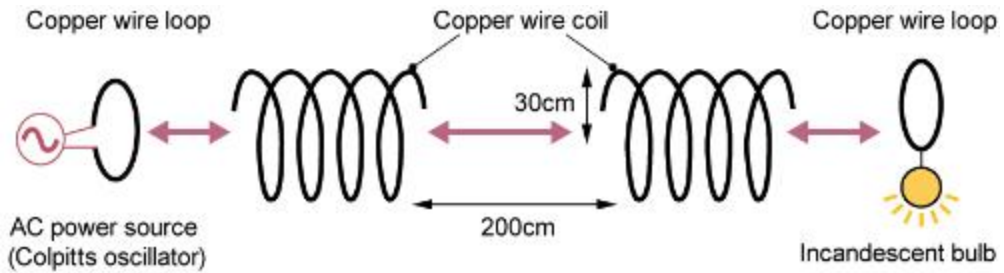
Fig. 2.4 Arrangement of coils to transfer power over a distance of 2m by MIT [14]

2.2.2 Formation of 'Qi' WPT standards

To enhance the versatility of WPT (compatibility of all devices with appropriate transmitters and receivers) and to reduce cost, the Wireless Power Consortium (WPC) issued an interface standard known as "Qi." This name (pronounced as "chee") is a Chinese word that means "air." Qi uses inductive power transfer and focuses on technology that transmits power to devices within close proximity to a charging station. Typical devices developed using Qi standards can power the devices over a distance up to 4 cm for low power-applications of about 5W using non-radiative technique [15]. The wireless charging system is comprised of a power transmission pad and a compatible receiver in the device. When a device is placed on transmission pad, the device is charged through inductive resonant coupling. Systems confirming to Qi standards will have output voltage regulated by means of a digital control loop in which the receiver communicates with the transmitter for more or less power using back scatter modulation, in which change in current at transmitter for a loaded receiver is monitored and demodulated into information required for devices to work together. In 2011, WPC extended the Qi standard for medium level power which is about 120W. Fig. 2.5 below shows the typical WPT application from wireless power consortium.

Fig. 2.5 Qi-standard wireless charging pad from Proxi charging multiple devices. [16]

The base acts as a transmitting pad, which receives power from an ac power supply. Receiver coils embedded into the devices receive power and charge mobile devices without use of cords or wires.

The Qi standard is capable of transferring power efficiently to multiple receivers/devices/loads as shown in Fig. 2.5 above. The wireless charging pad charges multiple mobile phones at same time. In initial stages of development of the Qi standard, a drawback with these systems was that they needed to be placed precisely in order to make an efficient charging system, but recently this drawback has been overcome [16].

The developments discussed above in sections 2.2.1 and 2.2.2 have all adopted Tesla's principle of near field (i.e., non-radiative) magnetic coupling and resonance for efficient power transfer without wires.

Wireless charging technology for portable electronic devices has reached the commercialization stage. Today, WPC consists of more than 209 companies (as members) worldwide that provide wireless charging for their products using Qi as the interface standard. Leading cellular companies like Samsung and Nokia are also providing wireless chargers that employ Qi standards.

2.2.3 Recent WPT products for mobile applications

Apart from Qi there are also other standards in WPT, such as Alliance for Wireless Power (A4WP), Powermat, and Cota. Companies like Intel, Fulton Innovation, Splashpower (later acquired by Fulton Innovation in 2008) and Qualcomm are developing wireless power products conforming to the A4WP standards.

In 2008 Intel demonstrated wireless illumination of a 60W light bulb on stage at Intel Developer Forum (IDF) [17]. Since then Intel showed their Wireless Resonant Energy Link (WREL) powering a laptop, computer without batteries or to play music through speakers without wires.

Figure (Fig. 2.6) below shows the design and arrangement for WPT from Intel in powering a light bulb of 60W at a distance of 70cm from transmitter. Intel's WREL can provide the stable electrical power to moving receivers that can be arranged almost in any orientation (can allow any angle up to 70 degrees) with respect to source within the constant region of 70cm from transmitter. An Adaptive auto-tuning algorithm has been used that allows efficiency of 70% even when the sender and receiver are not aligned parallel to each other.
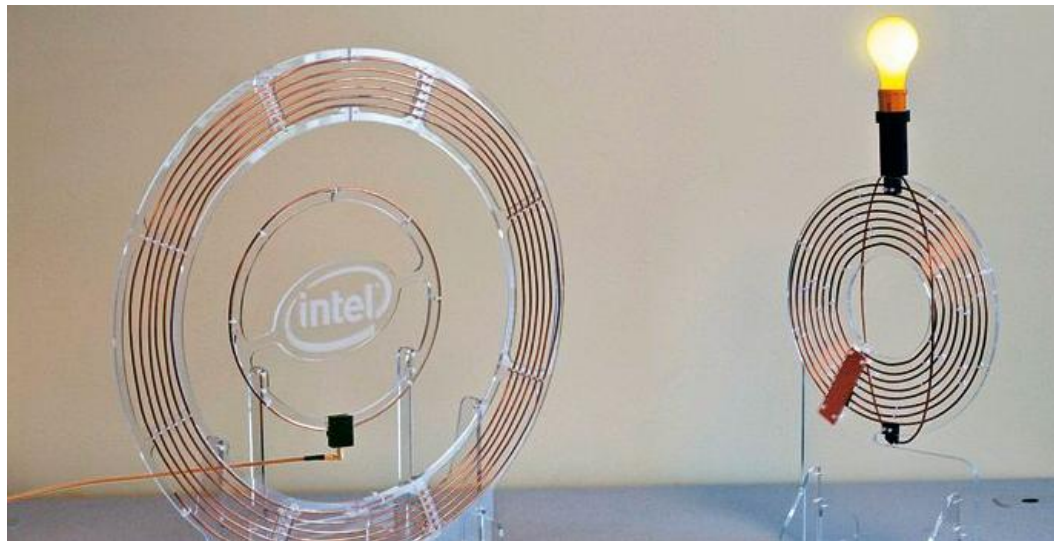
Fig. 2.6 Intel's demonstration of WPT [17]

Qualcomm is also introducing WPT applications where it has designed a mobile device charger that can be used to power mobile phones, tablets and a wide range of

applications using a resonance based method [18]. Fig. 2.7 below shows the demonstration of Qualcomm's WPT application.

Fig. 2.7 Qualcomm demonstrating WPT application [18]

It can be used to charge devices without direct contact and can power devices with different power levels simultaneously; metallic devices will not affect the charging process. Qualcomm is also is looking forward to get into revolutionary wireless charging of electric vehicles (EVs) which is discussed in a separate section.

There are various WPT systems like Powermat, Getpowerpad, Qualcomm's WiPower, Fulton and eCoupled conforming to WPC standards and use high frequency and thinner coils. All of these systems provide wireless charging for mobile devices using a mat (as transmitter) as shown in Fig. 2.5 and Fig. 2.7. As mentioned above, a system from Qualcomm which uses resonance based inductive coupling can transfer power up to a distance of 2ft (0.61m) and can be used to power or charge mobile devices like mobile phones, Bluetooth devices, and speakers, so forth within automobile. The next level of WPT applications is to power laptops, television receivers, home appliances, and similar devices. Various vendors are working on these developments. Fulton Innovation is working with commercial furniture manufacturers, designing applications for home and office uses.

2.2.4　Recent developments in WPT for electric vehicle (EV) applications

One of the important applications of high power application with WPT is rapid and efficient wireless charging of EVs. There are various companies such as Plug-less Power, Qualcomm (Halo IPT technology), Fulton, Tesla, and Hevo Power which are aiming to produce efficient wireless charging for EVs using inductive coupling. Charging units (chargers) of EV's are of large dimensions and transmitting antenna to charge it are relatively small, can send power up to 4-6in (10-15cm) from the ground to a receiver attached to the underside of the EV. When the EV is parked over the transmitter, the transmitter can charge the EV battery without the EV's being precisely placed over the transmitter [19]. Automatic algorithms are also being used to guide drivers to place EVs over the transmitter and can stop sending power if any obstacles come between the transmitter and receiver. Tesla Motors has already designed and employed rapid wired charging (for the Tesla Roadster) which can fully charge the EV in about 45-60min with 95% efficiency and is now working on implementing a wireless charging system. Fulton Innovation has designed a wireless charging system for EVs which could achieve an efficiency of approximately 80% (it predicts about 85% in theoretical efficiency).

In 2012 Qualcomm demonstrated wireless charging of EVs with their Halo IPT Wireless Electric Vehicle charging (WEVC) technology as in Fig. 2.8 below. These rapid charging systems operate in the range of kW using the inductive power transfer (IPT) method demonstrated at the London Consumer Electronics Show (CES) [20, 21]. The IPT system consists of two coils; one is in the ground (the base charging unit) and the other is embedded in the vehicle (the vehicle charging unit).   The battery of the EV may be charged even if the alignment of the coils is not optimal. Qualcomm is presently conducting trials of this system on more than 50EVs. According to [22] the frequency range used in this power transmission system was from 20kHz -140kHz with the power input from 3kW using a single-phase ac supply, 7kW using a 3-phase supply, or 18kW or higher for rapid charging. A setup using 3kW supply can fully charge the EV overnight.

Fig. 2.8 Qualcomm demonstration of its new wireless power transmission system for electric vehicles (EVs) at the London, Consumer Electronics Show (CES) [22]

Shown in Fig. 2.8 is a demonstration of WPT for EVs from Qualcomm which consists of a power source, power transmitting pad, power receiving pad and control unit to display the alignment of the coils.

2.3 Recent trends and applications in WPT with single source

Wireless power is technology which is changing the way people are leading their lives by offering new levels of convenience, mobility and safety. There are different ways of transferring power from transmitter point to receiver point such as (1) radio/microwaves; (2) lasers; (3) ultrasound; (4) inductive coupling; (5) coupled resonant circuits; and (6) capacitive coupling. Each method has its advantages and disadvantages. Resonant circuits (MCRC) method that is being used for mid-range distances (1-2m) with reasonable efficiency and potential for high power is magnetically-coupled resonant circuits in which both transmitter and receiving coils are resonant at the same frequency. In the following section there will be presented a discussion of research into MCRC WPT and means for improving their efficiency.

2.3.1 Review of prior research work

A brief literature survey reveals various previously-published papers which were useful in providing solutions for various issues such as enhancing distance, improving efficiency, increasing power, reducing losses, and modeling nonlinear loads in WPT systems with single loads. A discussion of WPT systems involving multiple sources and/or multiple loads will be presented in Chapter Four.

Zierhofer [23] demonstrated that the flux-coupling coefficient between magnetically-coupled coils can be enhanced by distributing turns of coils across the diameter rather than concentrating them at the circumference.
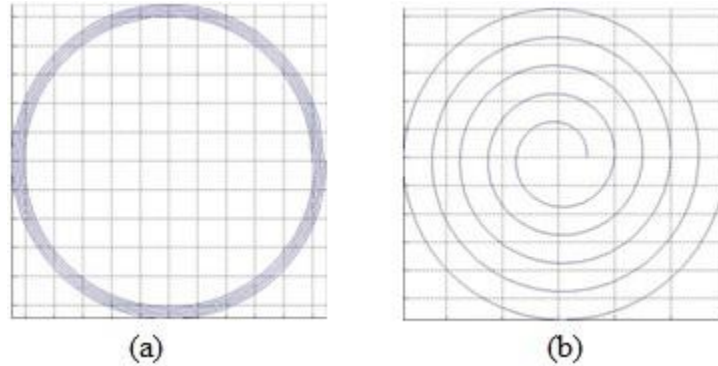
Fig. 2.9 (a) coil turns concentrated across circumference (b) coil turns distributed across diameter.

Kurs et al. [13] presented a model based on coupled mode theory (CMT). Their design included helical coils and was capable of delivering 60W over a distance of 2m with an efficiency of 40% while operating at 9.9MHz.

Kim et al. [24] investigated coupled-mode behavior of electrically-small meander antennas which demonstrated that high power efficiency can be achieved in the coupled-mode region of operation. An inductive load in the system will change the resonant frequency which will reduce the power transfer efficiency (PTE) of system.

Imura et al. [25] demonstrated a system with helical antennas for electric vehicles (EVs) to transfer power of about 100W over an air gap of 200mm at a frequency of 15.9MHz at an efficiency of 95% − 97%.

Beh et al. [26] described a study to improve the efficiency of MCRC WPT system with an impedance-matching technique. This work states that to achieve maximum efficiency in a WPT system, the resonant frequency of resonators and the operating frequency of system should be matched, an impedance matching network was used to adjust the resonant frequency of resonators to 13.56MHz which was the operating frequency. The impedance-matching network boosted efficiency from 50%–70%.

Ng et al. [27] demonstrated optimal design using a spiral coil for WPT systems with larger spacing between each turn and less number of turns which would improve the quality factor (Q) of the coils and hence improve efficiency of WPT system.

In 2010, Taylor et al. [28] demonstrated a wireless power station for laptop computers using magnetic induction which can deliver 32W of power to a laptop computer with a maximum efficiency of 60% at a frequency of 240 kHz. The system also had the ability to detect the presence of loads in order to reduce the no-load power consumption.

In 2011, Kim et al. [29] demonstrated a WPT system with intermediate resonant coil. Using an intermediate coil properly has enhanced the efficiency and distance between transmitter and receiver. System efficiency varied from 70%–85% with an intermediate coil placed in the system with a resonant frequency of 1.25MHz.

In 2011, Imura et al. [30] analyzed the relationship between maximum efficiency and air gap using the Neumann formula (a formula to calculate mutual inductance between pair of coils) and equivalent circuit model and proposed the equations for conditions required to achieve maximum power at given air gap.

In 2011, Lee and Lorenz [31] demonstrated a methodology of WPT system for multi-kW transfer over a large air gap using loose coupling between coils. This design delivered 3kW over an air gap of 30cm between transmitter and receiver with efficiency of 95% at a frequency of 3.7MHz. This work also discussed design of coils for higher Q.

Sample et al. [32] demonstrated a system with adaptive frequency tuning technique which compensates efficiency for variation in distance between transmitter and receiver. It demonstrated a constant efficiency over 70% for a constant-load receiver that can be moved to any position within a range of 70cm with resonant frequency of 7.65MHz.

Kim et al. [33] demonstrated an optimal design of a WPT system for an LED TV using multiple resonators. This system used a frequency of 250 kHz to transfer power of 150 W for a 47in (1.2m) LED TV with an efficiency of 80% for a separation of 20cm between resonators (transmitter and receiver).

Kiani et al. [34] demonstrated the circuit theory behind magnetically coupled resonant circuits and compared coupled-mode theory (CMT) with reflected load theory (RLT) and concluded both will result in the same set of equations in steady-state analysis while CMT is simpler as it reduces by 2 the order of differential equations when compared to RLT.

In addition to the work discussed above, there is also research taking place at the University of Texas at Tyler. In 2011, Beams and Annam [35] described a Matlab-based computational tool for calculating self- and mutual inductances for inductors of arbitrary shape and orientation in free space based on magnetic vector potential. Experimental measurements have validated the tool. In addition, an image method was introduced to compute inductances when coils are backed by sheets of high magnetic permeability (e.g., ferrite material).

Beams and Annam [36] also proposed a simplified method for designing four-coil resonant WPT network by sequential application of reflected impedances through mutual inductances. The design was verified by experimental validation.

In 2012, Annam [37] investigated a four-coil WPT system using resonant inductive coupling which proposed a design methodology of reflected impedances in loosely-coupled inductors in this method impedances are reflected sequentially through the inductors from load to source. The design was subjected to experimental validation and demonstrated efficiency exceeding 76% for various distances between transmitter and receiver.

Beams and Nagoorkar [38] investigated a theoretical design of a four coil MCRC WPT design that could transfer power over a distance of 2m with efficiency exceeding 70%, design yet has to be practically implemented.

Beams and Papasani [39] investigated a state-equation approach to model WPT network [20]. This approach permits termination of WPT networks with non-linear loads which is not possible with the usual phasor-transform network approach. This method

was simulated with a 3 coil WPT network and was compared with a verified model of the WPT network with resistive loads.

Chapter Three
Design and validation of a midrange WPT system
With a single source and load

In this chapter, the design and experimental validation of an MCRC WPT system with a single transmitter and receiver (load) that transfers power efficiently using non-radiative coupling is presented. The chapter begins with modification of the basic four-coil WPT system, followed by simulated design, and experimental design. Methods are described for measuring resonator parameters and flux-coupling coefficients between inductors. The chapter concludes with a summary of design validation.

3. 1 System and circuit topologies

The design presented in this section represents a departure from previous work. Unlike previous systems [36] the pickup coils which terminate with only a resistive load, a series capacitive component has been added to the make load coil resonant at the operating frequency, since with resistive termination; change in resistive loads will reflect only the resistive component, which avoids change of resonant frequency of the prior coils. The modified Basic circuit of 4-coil WPT is as shown in Fig. 3.1 below under Basic WPT system section.

3.1.1 Basic WPT system

The proposed midrange WPT system employs a four-coil topology rather than a two-coil topology. The four-coil system has greater flexibility with regard to impedance transformation than the two-coil system [36] and power can be transferred over greater distance with reasonable efficiency by the four-coil system than the two-coil system [40]. The circuit shown in Fig. 3.1 represents a typical modified four-coil WPT system.

The topology shown in Fig. 3.1 is consists of four inductors: driving coil L_1; transmitting resonator coil L_2; receiving resonator coil L_3; and load coil L_4. Four capacitors C_1–C_4 and a load resistance R_L complete the system. The system is energized by a square-wave source V_{sq}. Sinusoidal, steady-state analysis by means of the phasor transform may be applied to the circuit of Fig. 3.1 by decomposing the square-wave source V_{sq} into its harmonic components. For this type of analysis, V_{sq} is replaced by sinusoidal source v_s at the appropriate fundamental or harmonic frequency. In practice, the WPT network is designed such that the fundamental frequency of the square-wave source is the only constituent of the square wave that delivers significant power [36]. The output resistance of the driving square-wave source V_{sq} is R_s. Losses in each of the four loops are modeled by including equivalent series resistance (*ESR*) elements R_1–R_4. It is assumed that all four coils are coupled through mutual inductances M_{12}, M_{13}, M_{14}, M_{23}, M_{24}, and M_{34}. The principal (major) mutual inductances representing the direct path for power transfer are M_{12}, M_{23}, and M_{34}. The effect of the other mutual inductances (which may be termed *parasitic* mutual inductances) is to complicate the design and analysis process.
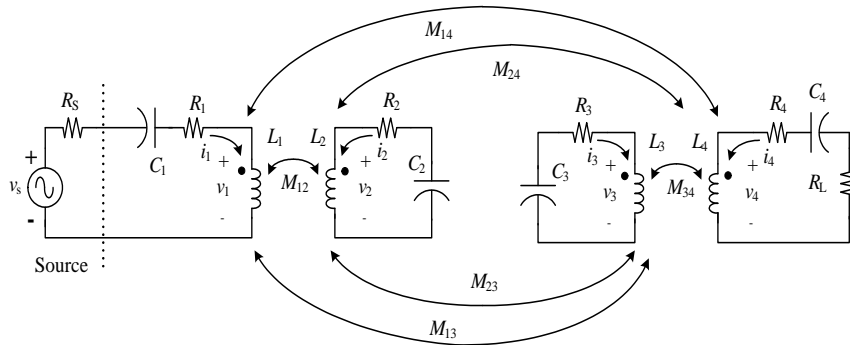
Fig. 3.1 Basic four-coil WPT system including loss elements and resistive load

Analysis of this circuit is straightforward if the appropriate component and parametric values are known *a priori*. Design is a much-more complex task due to the large number of degrees of freedom.

3.1.2 Design of a midrange WPT system

The goal of this design was a system capable of transmitting power over a nominal distance of 2m with an efficiency of at least 50% to a nominal load resistance of 5Ω. The operating frequency was chosen to be 100 kHz for the relative ease of realizing a square-wave source at this frequency. It was assumed that coils with Quality factor $(Q) \geq 200$ were practical at this frequency if wound with Litz wire. Coils designed for the system are single-layer spirals with a pitch (turn-to-turn spacing) of 0.015m for coils L_1 and L_4, while it is 0.01m for coils L_2 and L_3. The coils were designed with a large radius in order to improve their Q [40]. Coil data and computed self-inductances are as shown in Table 3.1 below. Identical coils were chosen for L_2 and L_3 to simplify the design process. Coils were designed with a Matlab application created by the University of Texas at Tyler that draws the inductors and computes their self-inductances by magnetic vector potential methods [35].

Table 3.1 Winding data and calculated self-inductance for the coils of the proposed midrange WPT system

Coil	Turns	Initial radius, m	Self Inductance, µH
L_1	5.25	0.5	65.77
L_2	32	0.275	1069.92
L_3	32	0.275	1069.92
L_4	1.25	0.5	6.89

The geometry of the circuit is shown in Fig. 3.2. Calculation of M_{23}, the mutual inductance of L_2 and L_3, gives 47.29µH and a flux-coupling coefficient k_{23} of 0.0442. The

condition for maximum distance and power transfer as suggested in [41, 42] is shown in Eq. (3.1) (excluding the parasitic coupling coefficients):

$$\frac{(k_{12} \cdot k_{34})}{(k_{23})} = 1 \qquad (3.1)$$

where k_{12} is the flux-coupling coefficient of L_1 and L_2 and k_{34} is the flux-coupling coefficient of L_3 and L_4. The separations of coils 1-2 and 3-4 shown in Fig. 3.2 were determined by simulation by calculating flux-coupling coefficients as the separations were varied. With the separations indicated, the calculated value of k_{12} at a separation of 0.3m was 0.2529 and k_{34} at a separation of 0.28m was 0.1913, giving a product of 0.0483, which is slightly larger than the calculated value of k_{23}.
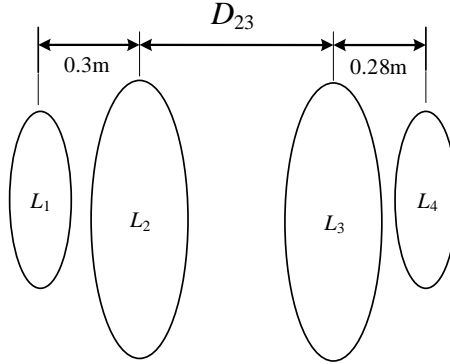
Fig. 3.2 Coil geometry of the proposed four-coil WPT system for midrange power transfer. The separation between transmitter resonator coil L_2 and receiver resonator coil L_3 is designated D_{23}. Its nominal value is 1m.

Magnetic vector potential methods were then applied to compute values for flux-coupling coefficients that vary with D_{23}. Table 3.2 below gives the results.

Capacitors C_2, C_3 and C_4 were chosen to resonate with L_2, L_3 and L_4, respectively, at the operating frequency of 100 kHz; their calculated values are 2.367nF for C_2, 2.367nF for C_3 and 367.639nF for C_4. In Fig. 3.1, Capacitor C_1 was chosen to be rather large to ensure that the input impedance of the WPT network would always retain a net inductive reactance.

Table 3.2 Coupling coefficients v/s D_{23}, separation between transmitter and receiver resonator coils

D_{23}, m	0.75	1	1.25	1.5	2
k_{13}	0.0366	0.0225	0.0146	0.0100	0.0052
k_{14}	0.0117	0.0073	0.0047	0.0031	0.0014
k_{23}	0.0800	0.0442	0.0264	0.0168	0.0079
k_{24}	0.0258	0.0157	0.0102	0.0069	0.0036

It has been found by experience and demonstrated by simulation that a load manifesting capacitive reactance can produce large shoot-through currents at switching transitions of the square-wave driver, possibly leading to its destruction [43].

The *rms* value of the fundamental component of the square wave driving the network was set to 45V and the output resistance of the square-wave drive was fixed at 0.3Ω; both values are reasonable for the application. The *ESRs* were estimated for all coils L_1-L_4 (assuming Q of 200 at 100 kHz) as $R_1 = 0.2066\Omega$, $R_2 = R_3 = 3.361\Omega$, and $R_4 = 0.0216\Omega$.

3.1.3   Simulation results of midrange WPT system

Table 3.3 below gives a summary of simulation results for input power, output power, and efficiency for cases: (i) with all coefficients and (ii) with major coefficients. The phase reference for all phase measurements is the input square wave; 0° is taken as the point of zero-crossing on a low-to-high transition of the input square wave.

From Table 3.3, it is clear that output power with a 1m transmitter-to-receiver separation is maximized (for case without parasitic coefficients), conforming to the expectations of Eq. (1). From Table 3.3, it can be seen that the results of all coefficients and major coefficients cases are almost similar indicating parasitic coefficients have negligible effects (except for spacing of 0.75m).

Table 3.3 Simulated input power, output power, and efficiency, for the four-coil midrange WPT network vs. D_{23} (separation of the transmitter and receiver resonator coils)

D_{23}, m	Input power, W		Output power, W		Efficiency, %	
	All co-efficients	Major co-efficients	All co-efficients	Major co-efficients	All co-efficients	Major co-efficients
0.75	33.7	22	25	16.4	74.2	74.4
1	32.9	28.9	24.8	21.8	75.4	75.4
1.25	17.6	17.5	11.9	11.8	67.4	67.3
1.5	9.8	9.8	5.2	5.2	52.8	52.7
2	5.1	5.2	1.2	1.2	22.8	22.8

The efficiency of the four-coil WPT system may also be estimated from reflected resistances, as given in Eq. (3.2) below [36] which can be derived using the network shown in Fig. 3.3
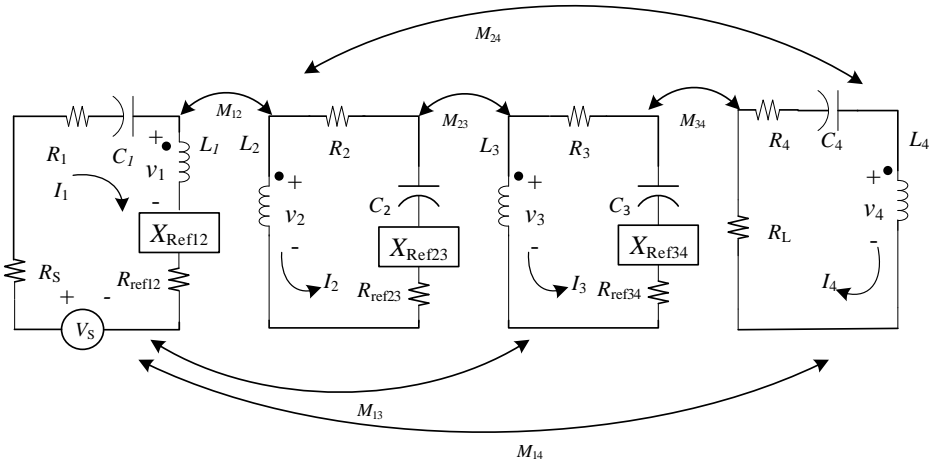
Fig. 3.3 Network to derive expression for efficiency shown in Eq. 3.2

$$\eta = \frac{R_L}{R_4 + R_L} \times \frac{R_{\text{ref}34}}{R_3 + R_{\text{ref}34}} \times \frac{R_{\text{ref}23}}{R_2 + R_{\text{ref}23}} \times \frac{R_{\text{ref}12}}{R_S + R_1 + R_{\text{ref}12}} \qquad (3.2)$$

where η is fractional efficiency (0–1.0), $R_{\text{ref}34}$ is the resistance reflected into L_3 from L_4, $R_{\text{ref}23}$ is the resistance reflected into L_2 from L_3, and $R_{\text{ref}12}$ is the resistance reflected into L_1 from L_2. The reflected resistance into coil x from coil y was computed by Eq. (3.3):

$$R_{\text{ref}xy} = \omega M_{xy}\left(\frac{|i_y|}{|i_x|}\right)\cos\left(\angle i_y - \angle i_x + 90°\right) \tag{3.3}$$

where ω is angular frequency of system; M_{xy} is mutual inductance between coil x and coil y; i_x is current in coil x, and i_y is current in coil y.

Computed reflected resistances and efficiencies from equations are shown in Fig. 3.4 below. The nearly-constant reflected resistance $R_{\text{ref}34}$ is unsurprising given the constant flux-coupling coefficient k_{34} and the relative isolation of L_4 from the other inductors except L_3.
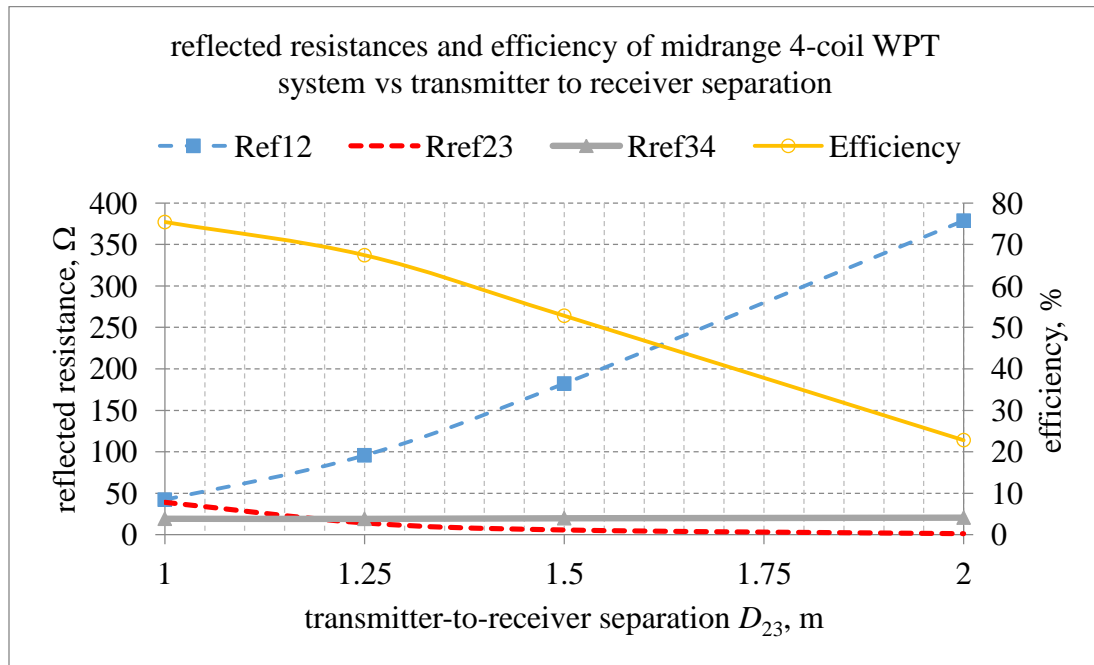
Fig. 3.4 Calculated reflected resistances computed with Eq. (3.3) and efficiency computed from Eq. (3.2) as a function of D_{23} (separation of transmitter and receiver resonators) in the four-coil WPT network

The effects of coil Q were also investigated for a nominal transmitter-to-receiver spacing of 1m. The resultant plot is shown in Fig. 3.5.
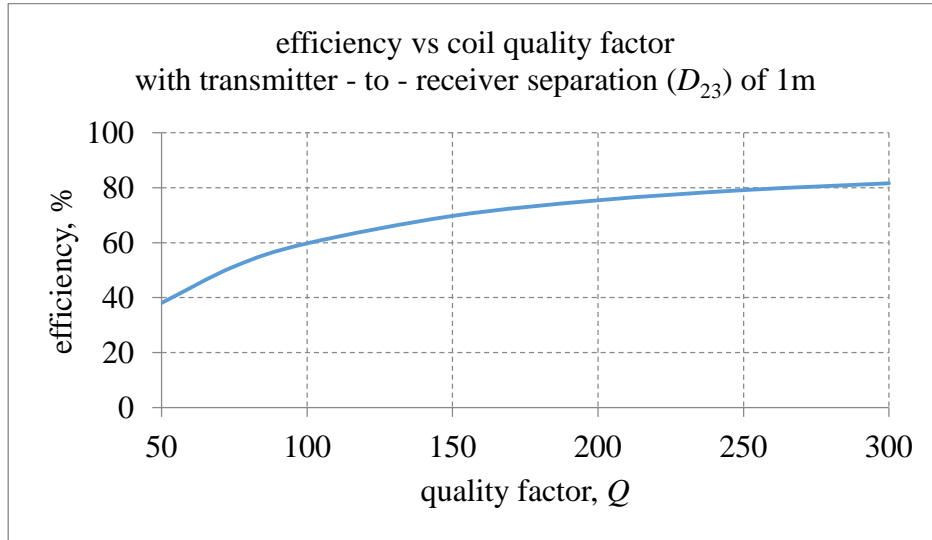
Fig. 3.5 Efficiency vs. inductor quality factor (Q) at a constant transmitter-to-receiver separation of 1m

The evident strong dependence of efficiency upon Q is expected.

3. 2 Empirical validation of design

3.2.1 Fabrication of coils

After designing and simulating the model to transfer power over a distance of 2m with reasonable efficiency, the design was realized for experimental validation. Coils were designed in spiral form to produce the inductances in Table 3.1, but practical implementation of spirals of such large size was difficult. Instead, octagonal coils approximating spirals were constructed using acrylic coil supports and spacers mounted on peg board. Coils were fabricated using Litz wire as it minimizes skin and proximity effects when operating at higher frequencies [41]. Three of the coils are shown in Fig. 3.6 below.
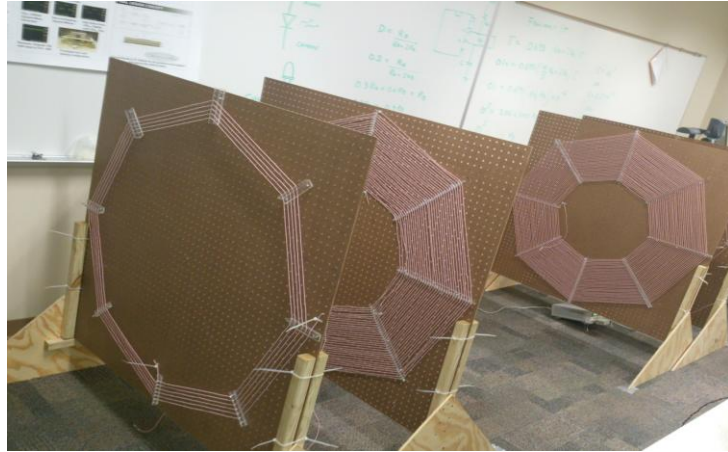
Fig. 3.6 Octagonal coils in approximation to spirals. Coils visible in this image are (left to right) L_1, L_2, and L_3

After designing the coils as shown above, self-inductance (L) and quality factor (Q) of the coils were measured at 100 kHz using the L_s (series L-R) measurement mode of an Agilent 4362 LCR Bridge. Readings are as shown in Table 3.4 below.

Table 3.4 Measured data for fabricated coils

Coils	Measured Inductance, μH	Measured Q	Calculated resistance, Ω
L_1	66.40	220	0.19
L_2	1053	410	1.6
L_3	1052	410	1.6
L_4	7.99	76	0.07

Measurement of L and Q of coils was performed with the coils oriented vertically and with their bottom edges elevated 20cm to avoid any effects due to the structural steel in the building floor. The accuracy of Q was limited by measurement capability of LCR Bridge.

3.2.2   Tuning coils to resonance

The WPT system design required resonating all inductors (except L_1) at the design resonant frequency (100kHz). Resonating inductors at 100kHz required precise adjustment of resonating capacitance so combinations of fixed film capacitors were used to bring the resonant frequency to slightly above 100kHz, and additional adjustable capacitance was supplied with a "sheet" capacitor fabricated from double-sided printed-circuit board material. Fig. 3.7 shows one such sheet capacitor. The side of the board visible in Fig. 3.7 is divided into 100 rectangular sections of 21mm × 29mm each; the reverse side is covered by a solid sheet of copper. The capacitance between each rectangular section and the backside sheet is approximately 24pF. Connecting rectangular sections in parallel allowed precise control of the resonating capacitance, Sheet capacitors like the one in Fig. 3.7 were used in resonating coils L_2, L_3 and L_4. An HP33120 Arbitrary Waveform Generator was used as a signal source for these tests.
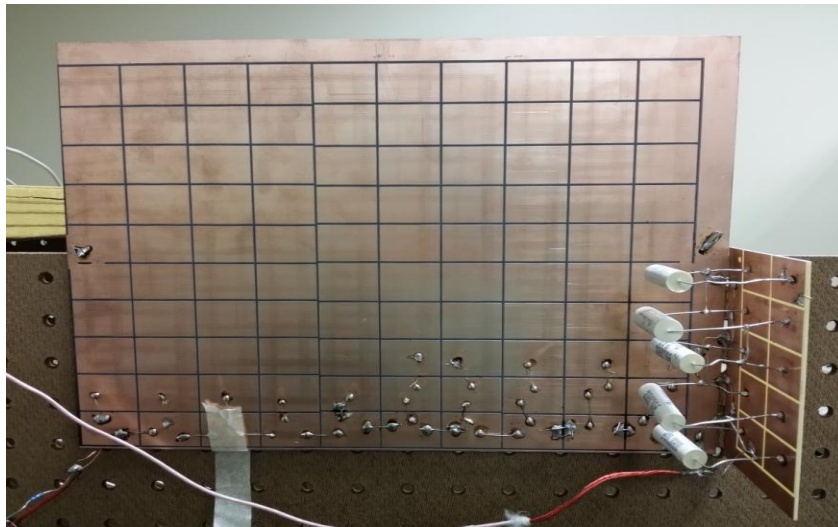
Fig. 3.7 Sheet capacitance used to adjust resonant frequency

3.2.3   Measurement of resonator parameters

Each of the four resonant circuits was characterized. Measured parameters included self-inductance (L), equivalent series resistance (ESR), and capacitance (C). The resonant frequency (f_r) for each resonant circuit (or resonator) was computed from the measured values of L and C. To obtain measured data, an LCR resonant circuit was

formed as shown in Fig. 3.8 below. A current sense resistance of 1Ω was installed in series with the resonant circuit, and an HP33120 Arbitrary Waveform Generator was used as a sinusoidal signal source. The generator had an additional output resistance of 50Ω, and it was adjusted to an open-circuited output voltage of 20Vpp. The voltage at the input of the resonator (v_{in} in Fig. 3.8) and voltage across the current-sense resistance (v_{oi} in Fig. 3.8) were measured using an Agilent DSO-2000X digital oscilloscope. Using the data acquired from oscilloscope, ratio of output voltage to input voltage was calculated using excel spreadsheet. Later, calculation of ratio of output voltage to input voltage and phase angles using Eqs. (3.4) and (3.5) shown below were determined.
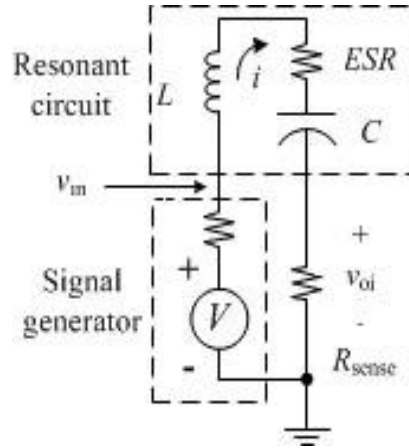
Fig. 3.8 Circuit for measurement of resonator parameters

$$\left| \frac{v_{oi}}{v_{in}} \right| = \frac{R_{\text{sense}}}{\left\{ (R_{\text{sense}} + ESR) + j\left(\omega L - \frac{1}{\omega C} \right) \right\}} \tag{3.4}$$

$$\angle \frac{v_{oi}}{v_{in}} = -\tan^{-1} \left[\frac{\left(\omega L - \frac{1}{\omega C} \right)}{R_{\text{sense}} + ESR} \right] \tag{3.5}$$

The measurement technique was as follows. The frequency of the signal generator was adjusted until v_{in} and v_{oi} were in phase at series resonance. *ESR* was computed using Eq. (3.6):

$$ESR = R_{\text{sense}} \left(\frac{1}{\left|\frac{v_{oir}}{v_{inr}}\right|} - 1 \right) \tag{3.6}$$

where v_{inr} is the voltage at the input of the resonator at resonance and v_{oir} is the voltage across the sense resistor at resonance. Then the generator frequency was varied in steps; at each measurement frequency, the magnitudes of v_{in} and v_{oi} and the phase angle of v_{oi} relative to v_{in} were measured. The error between measured phase and calculated phase at each frequency was computed with Eq. (3.7):

$$\varepsilon_\varphi(\omega) = \angle \frac{v_{oi}}{v_{in}} + \tan^{-1} \left[\frac{\left(\omega L - \frac{1}{\omega C}\right)}{R_{\text{sense}} + ESR} \right] \tag{3.7}$$

where $\varepsilon_\varphi(\omega)$ is the error between measured phase and expected phase at angular frequency ω. Parameters L and C were determined numerically to minimize the sum of the squares of the phase errors. Parameter values for respective resonant circuit are as shown in Table 3.5 below.

Table 3.5 Parameters L, ESR, C, measured by techniques outlined in Section 3.2.3, Resonant frequency f_r was calculated from measured values of L and C

Circuits	L, µH	C, nF	f_r, kHz	ESR, Ω	Q,, calc
$L_1 C_1$	69.024	219.42	40.8	0.270	160.6
$L_2 C_2$	1044.99	2.430	99.9	3.405	192.8
$L_3 C_3$	1055.75	2.400	99.9	3.806	174.3
$L_4 C_4$	8.00	313.86	100.4	0.175	28.7

3.2.4   Measurement of flux-coupling coefficients

Measurement of flux-coupling coefficients (k) was done between one pair of coils at a time. Other coils were open-circuited. The measurement circuit was as shown in Fig. 3.9 below.
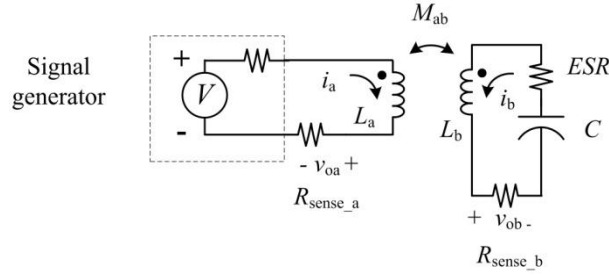
Fig. 3.9 Circuit for measurement of mutual inductance M_{ab} of inductors L_a and L_b where L_b is part of a series-resonant circuit. The signal generator was an Agilent HP33120A Aritrary Waveform Generator

A loop equation for the resonant circuit in Fig 3.9 gives:

$$(j\omega M_{ab} i_a) = -i_b \left(\frac{1 - \omega^2 L_b C}{j\omega C} + R_{sense\_b} + ESR \right) \qquad (3.8)$$

Where M_{ab} is mutual inductance between coil a and coil b.

Loop current i_a is determined by measuring the voltage across sense resistor R_{sense_a}. At resonant frequency ω_r:

$$\omega_r = \frac{1}{\sqrt{L_b C}}$$

Then Eq. (3.8) evaluated at ω_r gives:

$$(j\omega_r M_{ab} i_a) = -i_b (R_{sense\_b} + ESR) \qquad (3.9)$$

$$\omega_r M_{ab} |i_a| \angle i_a + 90° = (R_{sense\_b} + ESR)|i_b| \angle 180° \qquad (3.10)$$

From Eq. (3.10), it can be seen that current i_a must lead i_b by $+90°$ at ω_r. Thus resonance in the $L_b C$ circuit may be determined by locating the frequency at which i_a and i_b are in quadrature. Then the mutual inductance M_{ab} between L_a and L_b may be computed by:

$$M_{ab} = \left| \frac{i_b}{i_a} \right| \frac{(R_{sense\_b} + ESR)}{\omega_r} \tag{3.11}$$

Actual measurements were made with an HP33120 Arbitrary Waveform Generator as the signal source. The generator was set to produce a sinusoid with an open-circuit voltage of 20Vpp. The output resistance of the HP33120A is 50Ω. Current-sense resistors were 10Ω carbon-film. The flux-coupling coefficient k_{ab} between L_a and L_b was computed by Eq. (3.12). This procedure was

$$k_{ab} = \frac{M_{ab}}{\sqrt{L_a L_b}} \tag{3.12}$$

followed to calculate k_{12}, k_{23}, and k_{34}. Flux-coupling coefficients k_{13}, k_{14}, k_{24} were neglected as they are expected to have little effect as shown in Section 3.1.3. Table 3.6 below shows the simulated and measured flux-coupling coefficients for $D_{23} = 1m$ and 2m.

Table 3.6 Simulated and measured coupling coefficient (k) at different separations D_{23} between L_2 and L_3

Coupling coefficient (k)	$D_{23} = 1.0m$		$D_{23} = 2.0m$	
	Simulated	Measured	Simulated	Measured
k_{12}	0.2529	0.2322	0.2529	0.2332
k_{23}	0.0442	0.03741	0.0079	0.00756
k_{34}	0.1913	0.1919	0.1913	0.1919

Comparison of measured flux-coupling coefficients and simulated flux-coupling coefficients in Table 3.6 shows there is a slight discrepancy. It is not unexpected, however, as the calculation of flux-coupling coefficients assumes the coils to be spirals but the actual coils were octagonal.

3.2.5 Measurements of electrical performance

Measured electrical performance parameters were the input current, input voltage, and output power at the load. To measure the input current, a sense resistor of 1Ω was installed in series with coil L_1 (which could be accommodated in simulation by adding 1Ω to the *ESR* of L_1). A square-wave driver circuit with an output resistance on the order of 0.1Ω was used to drive the system. The driver circuit was itself driven with a square wave at 100.0kHz supplied by an Agilent 33120A Arbitrary Waveform Generator. A variable supply of up to 100V allowed the square-wave driver to produce up to a 100Vpp signal. Using an Agilent DSO-2000X digital oscilloscope, the current through coil L_1 (determined from measured voltage across the current-sense resistor) and voltage across coil L_1 were acquired. The phase reference for all measurements was taken at the point of zero crossing on a low-to-high transition of the input square wave. Digitized waveform data were acquired by the oscilloscope and transferred to Excel for analysis. In the case of current I_1 through L_1 and the voltage across coil L_1, the waveforms were non-sinusoidal. These waveforms were decomposed into their fundamental and harmonic components by numerical determination of amplitude and phase parameters of the Fourier-series representation of the original waveform.

Once the Fourier-series parameters of the input voltage and input current waveforms were determined, the input power could be determined by Eq. (3.13) below

$$P_{in} = \frac{|v_1||i_1|}{2} cos(\angle v_1 - \angle i_1) + \frac{|v_2||i_2|}{2} cos(\angle v_2 - \angle i_2) + \cdots + \frac{|v_n||i_n|}{2} cos(\angle v_n - \angle i_n)$$

$$\dots \quad (3.13)$$

where $|v_n|$ is the amplitude of the nth harmonic of the input voltage (including the fundamental component, for which $n=1$), $|i_n|$ is the amplitude of the nth harmonic of the input current, $\angle v_n$ is the phase of the nth harmonic of the input voltage, and $\angle i_n$ is the phase of the nth harmonic of the input current. In most cases, there will be very little power delivered by any frequency component except the fundamental, and the input power may be computed as below

$$P_{in} \approx \frac{|v_1||i_1|}{2} cos(\angle v_1 - \angle i_1) \qquad (3.14)$$

where $|v_1|$ and $|i_1|$ are amplitudes of voltage and current, respectively, and $\angle v_1$ and $\angle i_1$ are the phase angles of voltage and current, respectively, of the fundamental components of the input voltage and current waveforms.

Voltages across coils L_2, L_3 and L_4 were measured. These voltages were sinusoidal in nature as would be expected from resonant circuits of high Q. Output power was measured using the measured voltage across non-inductive resistive load (R_L) value at coil L_4 using the Eq. (3.15) shown below.

$$P_{Out} = \frac{V_{rms}^2}{R_L} \qquad (3.15)$$

where V_{rms} is the *rms* voltage across load resistor R_L. Measured results are summarized in Table 3.8 below. Table 3.8 below shows measured and simulated data for input power, output power, and efficiency at distances D_{23} of 1m and 2m between the transmitting and receiving resonators. Measurements for D_{23}=1m were acquired when system was excited with 100Vdc supply, while for D_{23}=2m, the system was excited with 50Vdc supply. Measurement of the input power for the network at spacing D_{23} of 2m was not performed by Fourier decomposition of the input voltage and current waveforms, but was rather determined as the product of dc bus voltage to the square-wave driver and dc supply current. For these measurements, the dc bus voltage was supplied by an Agilent E3631A DC power supply.

Table 3.7 Measured output power, efficiency, and input current (magnitude and phase) for the four-coil midrange WPT network vs. D_{23}, separation of the transmitter and receiver resonator coils

D_{23}, m	Dc Bus Voltage, V	Input power, W		Output power, W		Efficiency, %	
		Measured	Simulated	Measured	Simulated	Measured	Simulated
1	100	35.07	28.9	24.75	21.8	71	75.4
2	50	1.3	1.290	0.364	0.294	18	22.8

Performance of system was close to what simulation has predicted. The reason for slight drop of efficiency at both distances is the actual quality factor (Q) recorded is lower than value used in prediction.

3.3 Summary

In this chapter, the design of a four-coil magnetically-coupled resonant circuit WPT system with a single transmitter and single load was investigated. This system has been validated with both experimental and simulated data which agree within ±5%. Methodologies for measuring resonator parameters (self-inductance (L), capacitance (C), equivalent series resistance (ESR), and flux-coupling coefficients (k)) were presented. A method of measurement of input power by Fourier series decomposition has been demonstrated.

Chapter Four

Modeling of WPT system with multiple sources and loads

4.1 Summary of recent work in WPT with multiple sources and receivers

WPT systems with single loads have been discussed and demonstrated to transfer power over a mid-range (1-2m) with power ranging from mW to kW with reasonable efficiency using non-radiative coupling, loosely-coupled inductors and resonating capacitors. This chapter is intended to discuss and demonstrate the performance of WPT systems with multiple transmitters and/or multiple loads or receivers.

For over a decade, WPT systems using near-field (non-radiative) coupling with single loads (receivers) have been found to be attractive with good efficiency and power levels for reasonable distances. However, recent work in magnetically-coupled WPT systems includes multiple transmitters and multiple receivers. Some of recent developments of WPT systems using this type of topology are discussed below.

In 2010, Kurs et al [44] demonstrated power transfer to multiple devices. Demonstration with one source found powering two devices simultaneously resulted in increased overall efficiency even with relatively lower flux-coupling coefficients with individual devices.

In 2010, Kim et al [45] analyzed wireless energy transferred to multiple devices using CMT (coupled-mode theory) which states that efficiency of a multiple-receiver system is dependent on coupling coefficients between the source and loads and on the coupling coefficient between multiple loads systems and for reasonable efficiency of system one should be limited with number of receivers included in system.

In 2011, Bong [46] investigated design with variety of transmitter and receiver combinations WPT for improving power transfer efficiency (PTE). This was followed by a Monte Carlo simulation which predicts the optimum number of transmitters and

receivers for improving PTE of the system.

In 2012, Kim et al [47] described a compact planar structure which has multiple self-resonators (a total of 5) with a single load in which the position of the load can be varied over a region in which the receiver will couple with any one of the resonators. By varying the resonant frequency of the load coil the efficiency of the system was improved.

In 2013, Ahn and Hong [48] investigated a WPT system with multiple transmitters and multiple receivers. Frequency conditions for maximum efficiency and power are addressed under flux coupling coefficient (k) with multiple transmitter and receivers placed in a limited space which include cross coupling coefficient (flux-coupling coefficient (k) between multiple transmitters and multiple receivers) also. Automatic adjustment of operating resonant frequency of system is provided. Power transfer of 51W−65W with efficiency between 45%−57% under very low flux-coupling coefficients of 0.025-0.063 was demonstrated.

In 2013, Shin et al [49] investigated high power application of a WPT system. A system with six supply and receivers pairs to obtain high power output is proposed using magnetically coupled resonance method. Power of 490kW was transferred over an air gap of 11cm with an efficiency of 90% at a frequency of 20 kHz.

In 2013, Lee et al [50] proposed a new topology suitable for dynamic wireless charging. The system consists of a transmitter and multiple coils commensurate with moving receivers. It uses reflected reactance by receiver in to transmitter to automatically increase the field strength between transmitter and receiver and reach maximal efficiency. The system operated at 100 kHz with a total output power of 300W.

4.2 Design tool for WPT system comprising multiple transmitter (source) and/or receivers (loads)

A major design consideration for commercial application of WPT is the space or region in which a device may be placed for drawing power without use of cords or cables [12]. In this section, a discussion is presented of a WPT design with multiple resonators, each of which may be used as a power source (transmitter), passive resonator, or power sink (load or receiver) which may enhance the region over which device can be placed

for drawing power wirelessly. A calculation tool using Excel has been developed to estimate the performance of multiple-resonator WPT networks.

4.2.1   Development of a universal resonator block

The circuit shown below in Fig. 4.1 is a basic resonant circuit with an inductor (L), a capacitor (C), and a resistance (R_{ESR}, the sum of equivalent series resistances of L and C), as the basic components.
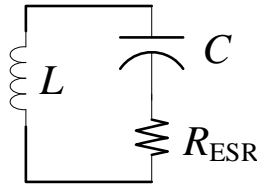
Fig. 4.1 Basic passive resonator of a generic WPT system

The passive resonator can be transformed into a receiver (load) by adding a load resistance R_L as shown in Fig. 4.2(a); it can be transformed into transmitter (source) by adding a voltage source V_s with an output resistance R_s and output inductance L_s as shown in Fig. 4.2(b); and it can be used as a passive/self-resonator without adding any other components. A square-wave source is used in practice as voltage source V_s. An output inductance L_S is included in series with the source for mitigation of the possibility that the impedance connected to the terminals of V_s might become capacitive under certain loading conditions. Driving a capacitive load with a square wave driver may result in destruction of the driver [43]; in most circumstances, however, it is expected that L_S will be zero.

Combination of the source resonator and the receiver resonator will result in formation of universal resonator block as shown in Fig. 4.3 that can be used to fulfill any role (as source, load/receiver, passive/self-resonator) as needed by proper choice of components and parameters.
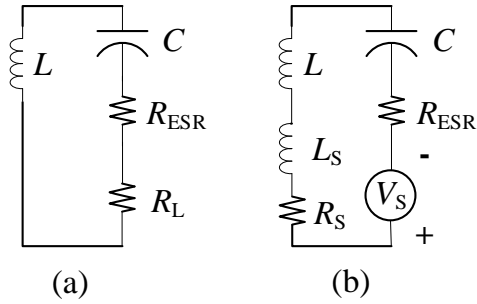
Fig. 4.2 (a) and (b): Transformation of the basic passive resonator into a receiver (a) and a transmitter (b)
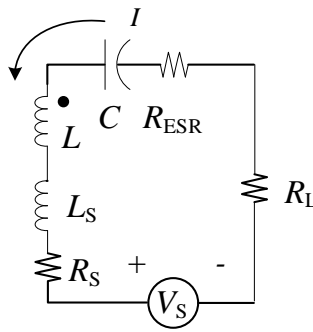
Fig. 4.3 Universal resonator block. The reference polarity of the inductor and direction of current I have been added

4.2.2 Analysis of a WPT network composed of universal resonator blocks

A WPT network composed of n universal resonator blocks is diagrammed in Fig 4.4 below.
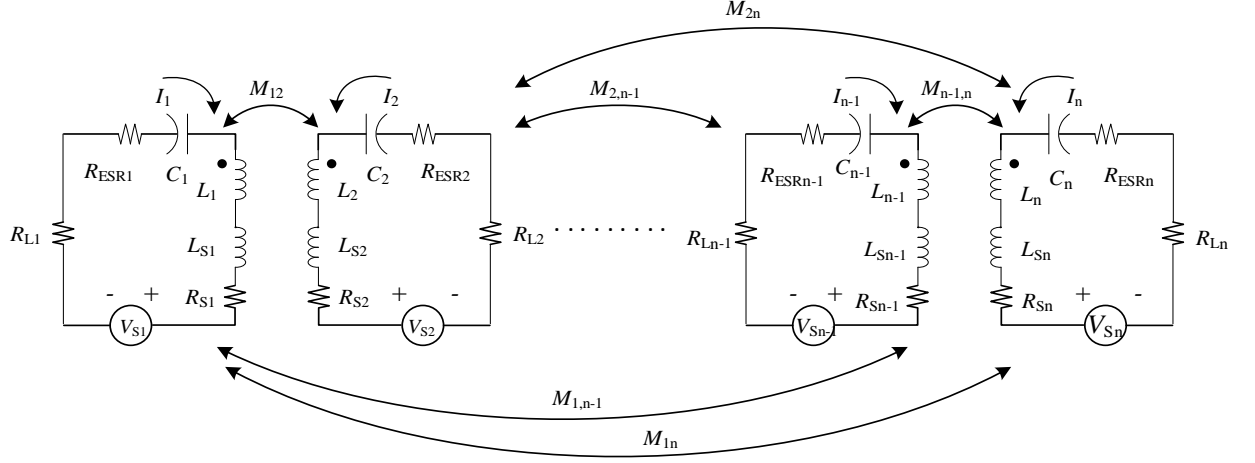
Fig. 4.4 WPT system with multiple resonators

The resonators are linked through mutual inductances M_{12}, M_{13}….. $M_{(n-1),n}$. A loop equation may be written for each resonator, and these loop equations may be solved simultaneously. Loop equations are given below for the network of Fig. 4.4 under sinusoidal, steady state excitation at angular frequency ω:

$$-V_{s1} = I_1(R_{s1} + R_{ESR1} + R_{L1}) + j\left[\omega(L_{s1} + L_1) - \frac{1}{\omega C_1}\right]I_1 \ldots$$

$$+j\omega M_{12}I_2 + j\omega M_{13}I_3 + \ldots +j\omega M_{1n}I_n$$

$$-V_{s2} = I_2(R_{s2} + R_{ESR2} + R_{L2}) + j\left[\omega(L_{s2} + L_2) - \frac{1}{\omega C_2}\right]I_2 \ldots$$

$$+j\omega M_{12}I_1 + j\omega M_{23}I_3 + \ldots +j\omega M_{2n}I_n$$

$$.$$
$$.$$
$$.$$

$$-V_{sn} = I_n(R_{sn} + R_{ESRn} + R_{Ln}) + j\left[\omega(L_{sn} + L_n) - \frac{1}{\omega C_n}\right]I_n \ldots$$

$$+j\omega M_{1n}I_1 + j\omega M_{2n}I_2 + \ldots +j\omega M_{(n-1)n}I_{n-1} \tag{4.1}$$

These equations can be expressed in a matrix form as shown below:

$$
\begin{bmatrix}
\left(R_1 + j\omega L_1 + \dfrac{1}{j\omega C_1}\right) & (j\omega M_{12}) & (j\omega M_{13}) \dots (j\omega M_{1n}) \\
(j\omega M_{12}) & \left(R_2 + j\omega L_2 + \dfrac{1}{j\omega C_2}\right) & (j\omega M_{23}) \dots (j\omega M_{2n}) \\
& \vdots & \\
(j\omega M_{1n}) & (j\omega M_{2n}) & (j\omega M_{3n}) \dots \left(R_n + j\omega L_n + \dfrac{1}{j\omega C_n}\right)
\end{bmatrix}
\begin{bmatrix} I_1 \\ I_2 \\ \vdots \\ I_n \end{bmatrix}
=
\begin{bmatrix} V_{s1} \\ V_{s2} \\ \vdots \\ V_{sn} \end{bmatrix}
\qquad (4.2)
$$

where $R_1', R_2', \dots, R_n'$ represent the sums of all resistances ($R_n' = R_{sn} + R_{ESRn} + R_{Ln}$) in each resonator; $M_{1n}, M_{2n}, \dots M_{(n-1)n}$ are mutual inductances; $L_1', L_2', \dots L_n'$ are sum of inductances ($L_n' = L_{sn} + L_{ESRn}$) in each resonator; $C_1, C_2, \dots C_n$ are the capacitances in each resonator; $I_1, I_2, \dots I_n$ are currents in each resonator; $V_{s1}, V_{s2}, \dots V_{sn}$ are the supply voltages in each resonator.

Eq. (4.1) may be solved using tools such as Excel or Matlab in a relatively straightforward manner. An Excel spreadsheet calculator for analysis of multiple-resonator WPT systems has been developed to solve the loop equations for networks of up to eight resonators. Input parameters for each resonator include the source voltage V_s; phase of the source voltage; resonator inductance (L); source resistance (R_s); source inductance (L_s); inductor ESR (ESR_L), capacitance (C); ESR of the capacitance (ESR_C); and load resistance (R_L). Flux-coupling coefficients ($k_{12} \dots k_{78}$) are also supplied by the user. Individual resonators may be excluded from the network if a WPT network of fewer than eight resonators is to be represented. This spreadsheet predicts the performance of the system by computing current in each resonator, voltage across each resonator's inductor, input power to each source (transmitter) resonator, and output power at each load resistance. Losses in each resonator, as well as overall efficiency, are computed. A Matlab script has been written to validate the calculations of the spreadsheet.

4. 3 Design of a multi-resonator WPT system with one transmitter and two receivers

A 5-resonator system with one transmitter, two passive resonators, and two receivers has been designed, analyzed with the Excel WPT design tool, constructed, and tested.

4.3.1　System and circuit topology

The proposed mid-range WPT system with multiple resonators employs five resonators as in Fig. 4.5. They are the transmitting resonator (including L_1); passive resonator (including L_2); receiving resonator (including L_3); and receiver (load) resonators including L_4 and L_5. Five capacitors C_1–C_5 and two load resistances R_{L4} and R_{L5} composed non-inductive thick-film power resistors complete the system. The system is driven by a square-wave source V_{s1} in resonator 1. It is assumed that voltage source V_{S1}
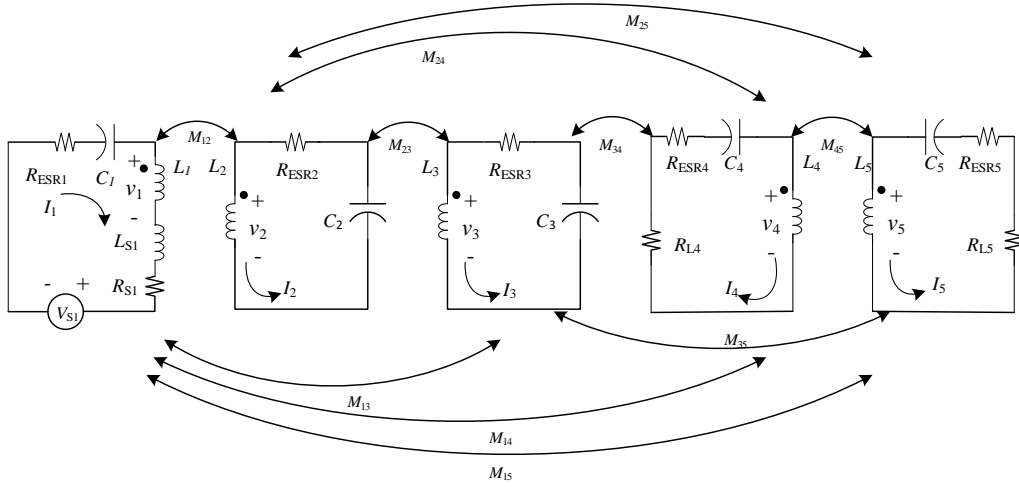
Fig. 4.5 Schematic of five-resonator WPT system with one source and two loads.

produces a square wave. However, sinusoidal steady-state analysis by means of the phasor transform may be applied to the circuit of Fig. 4.5 by decomposing the square-wave source into its harmonic components. For this type of analysis, V_{S1} is replaced by sinusoidal source v_s at the appropriate fundamental or harmonic frequency. In practice, the WPT network is designed such that the fundamental frequency of the square-wave source is the only constituent of the square wave that delivers significant power [36]. The output resistance of the driving square-wave source V_{S1} is R_{S1}. Losses in each of the five loops are modeled by including equivalent series resistance (ESR) elements R_{ESR1}–R_{ESR5}. It is assumed that all five resonators are coupled through mutual inductances M_{12}, M_{13}, M_{14}, M_{15}, M_{23}, M_{24}, M_{25}, M_{34}, M_{35} and M_{45}. The principal mutual inductances representing the direct path for power transfer are M_{12}, M_{23}, M_{34} and M_{35}. The effect of the other mutual inductances (which may be termed *parasitic* mutual inductances) is to complicate the design and analysis process.

4.3.2 Design of WPT system with five resonators

The design of five coil system is relatively straightforward, and its design process is similar to that described in Section 3.2.1, except that the single load was replaced with two new load resonators (which include L_4 and L_5). Coils L_4 and L_5 were designed as identical 10-turn single-layer spiral structures with a pitch (turn-to-turn spacing) of 0.015m and an initial (inner) radius of 0.14m. The calculated self-inductance of each coil was 55.56μH.

Linear separation between resonators in this design is same as the separation described in Section 3.2.4. The two load resonators replaced the resonator L_4-C_4 of the previous design. Magnetic vector potential methods were then applied to compute values for flux-coupling coefficients among the pairs of resonator inductors for D_{23} =1m. Flux-coupling coefficients k_{12}, $k_{13,}$ and k_{23} were assumed to be unchanged from their previous values. Table 4.1 below gives the calculated flux-coupling coefficients related to L_4 and L_5.

Table 4.1 Coupling-coefficients related to resonators L_4 and L_5

Resonator	1	2	3	5
4	0.00450	0.00829	0.10687	0.03150
5	0.00450	0.00829	0.10687	

Capacitors C_2, C_3, C_4 and C_5 were chosen to resonate with L_2, L_3, L_4 and L_5, respectively, at the operating frequency of 100.0 kHz; the calculated values for C_2 and C_3 are 2.367nF, while those for C_4 and C_5 were 45.469nF. Capacitor C_1 was chosen to be rather large as discussed under Section 3.1.2.

The *rms* value of the fundamental component of the square wave driving the network was set to 6.08V (consistent with a square wave source of 13.5Vpp) and the output resistance of the square-wave drive was fixed at 0.3Ω; both values are reasonable for the application. The *ESRs* were calculated (assuming Q of 200 at 100 kHz) as R_1 = 0.2066Ω, $R_2 = R_3 = 3.361$Ω, and $R_4 = R_5 = 0.175$Ω.

4.4 Construction and test of WPT system with five resonators

4.4.1   Fabrication of new load resonators for the five-resonator system

The five-resonator WPT system was constructed to validate experimentally the model described in Section 4.3.2. Resonators L_4 and L_5 were fabricated by winding them on acrylic coil supports attached to peg board as discussed in Section 3.2.1. The fabricated coils L_4 and L_5 are shown in Fig. 4.6 below. Fig. 4.7 shows the arrangement of resonators for experimental validation

Fig. 4.6 Fabricated resonators L_5 (left) and L_4 (right). The circuit board between the two coils is a load block consisting of nine clusters of 50Ω noninductive power resistors which could be combined to form various resistance values. At the center of each coil are found fixed capacitors and sheet capacitors for precise resonator tuning.
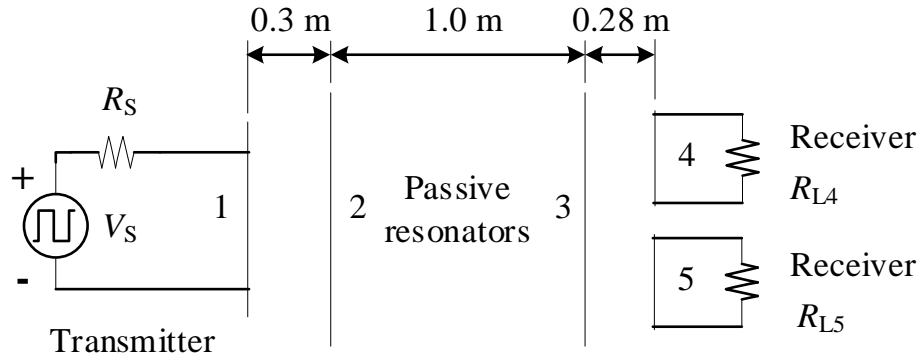
Fig. 4.7 Diagram of resonator arrangement of the five-resonator network with two receivers (loads) and a single transmitter (source), Numbers indicate resonator numbers.

After having fabricated coils L_4 and L_5 in Fig. 4.6, resonators were constructed by adding capacitors and load resistors. Capacitance values were chosen to resonate coils L_4 and L_5 at 100.0kHz. Fine-tuning of the resonant frequencies of each resonator was accomplished with "sheet" capacitors as discussed in Section 3.2.2.

4.4.2 Measurement of resonator parameters

A parameter-characterization test was performed on all resonators. The measurement methodology was the same as discussed in section 3.2.3. Below Fig. 4.8 – Fig. 4.12 show the plots of measured and calculated values of $\left|\frac{v_{oi}}{v_{in}}\right|$ and $\angle\left(\frac{v_{oi}}{v_{in}}\right)$ vs. frequency which were obtained during the process of resonator characterization.
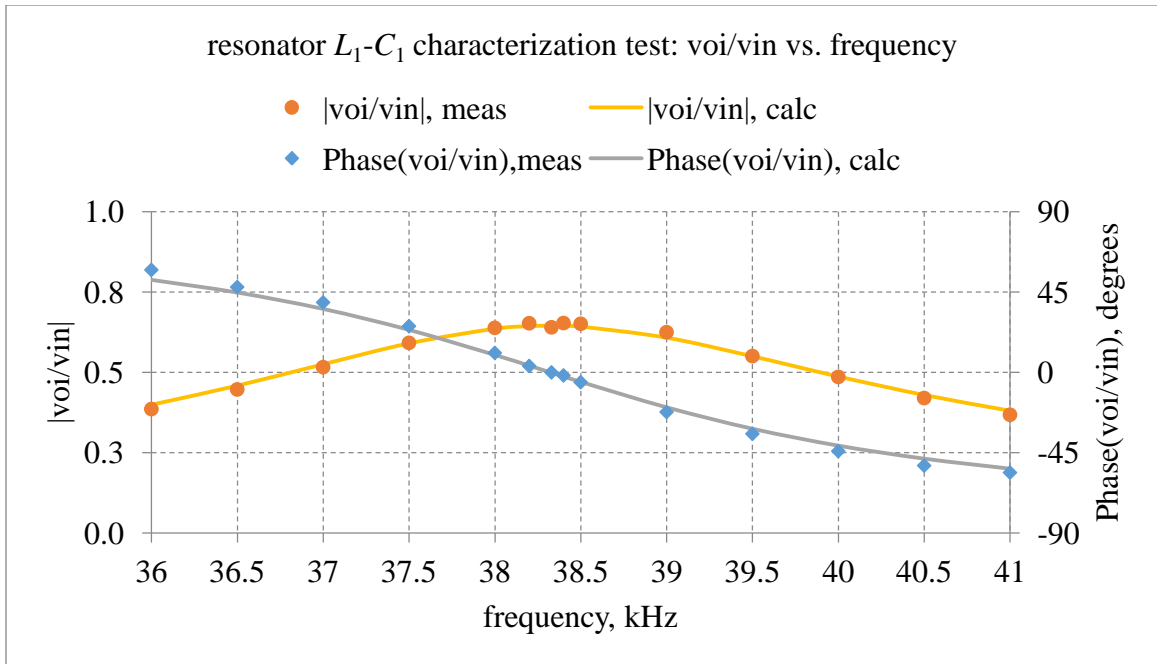
Fig. 4.8 Characterization of L_1-C_1 resonator Values of L_1=67.308 µH, C_1=256.3 nF, R_{ESR1}=0.566Ω provided the best fit of measured and calculated values
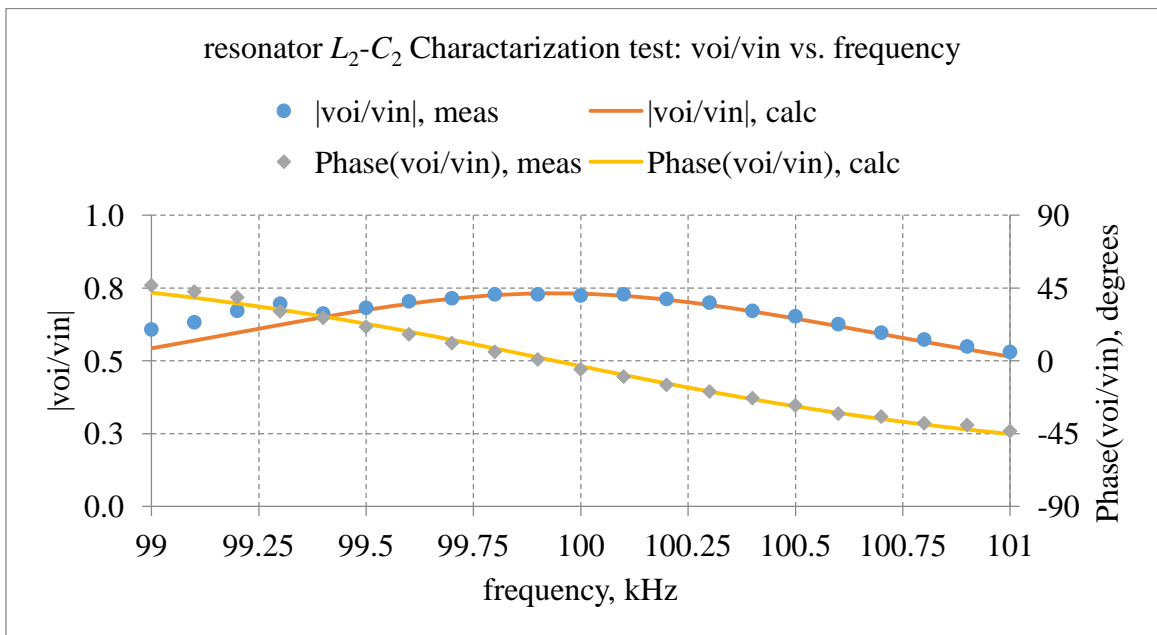
Fig. 4.9 Characterization of L_2-C_2 resonator Values of L_2=1040.18 µH, C_2=2.438 nF, R_{ESR2}=3.663Ω provided the best fit of measured and calculated values
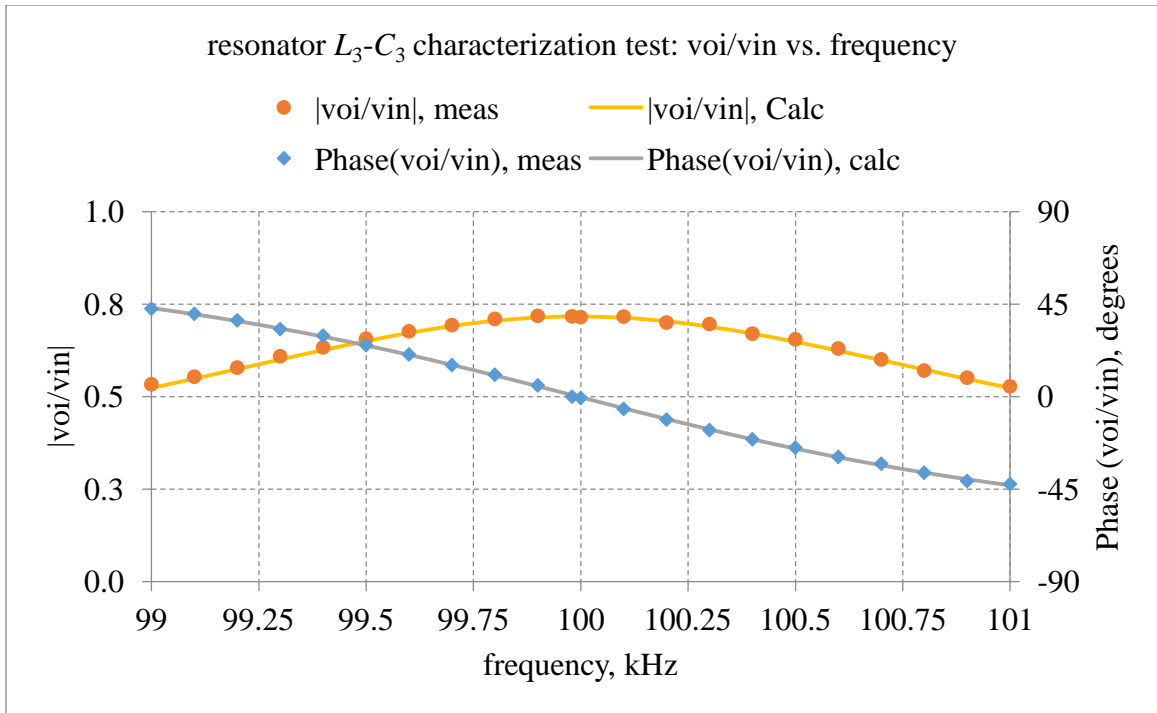
Fig. 4.10 Characterization of L_3-C_3 resonator Values of L_3=1044.99 µH, C_3=2.418 nF, R_{ESR3}=3.846Ω provided the best fit of measured and calculated values
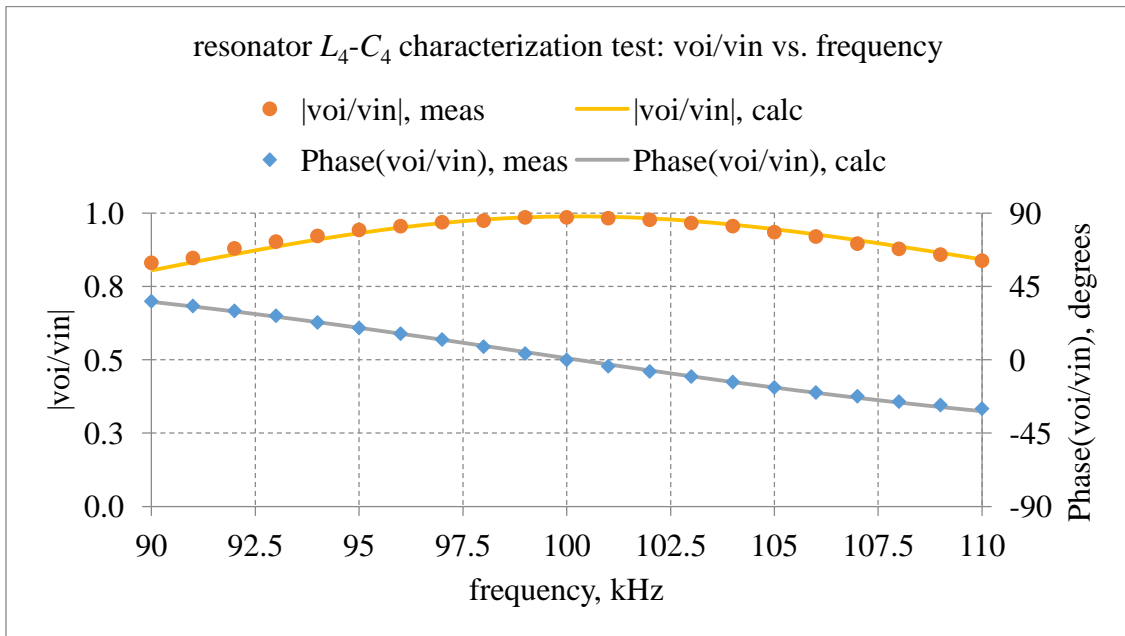
Fig. 4.11 Characterization of L_4-C_4 resonator Values of L_4=53.17 µH, C_4=47.409 nF, R_{ESR1}=0.111Ω provided the best fit of measured and calculated values
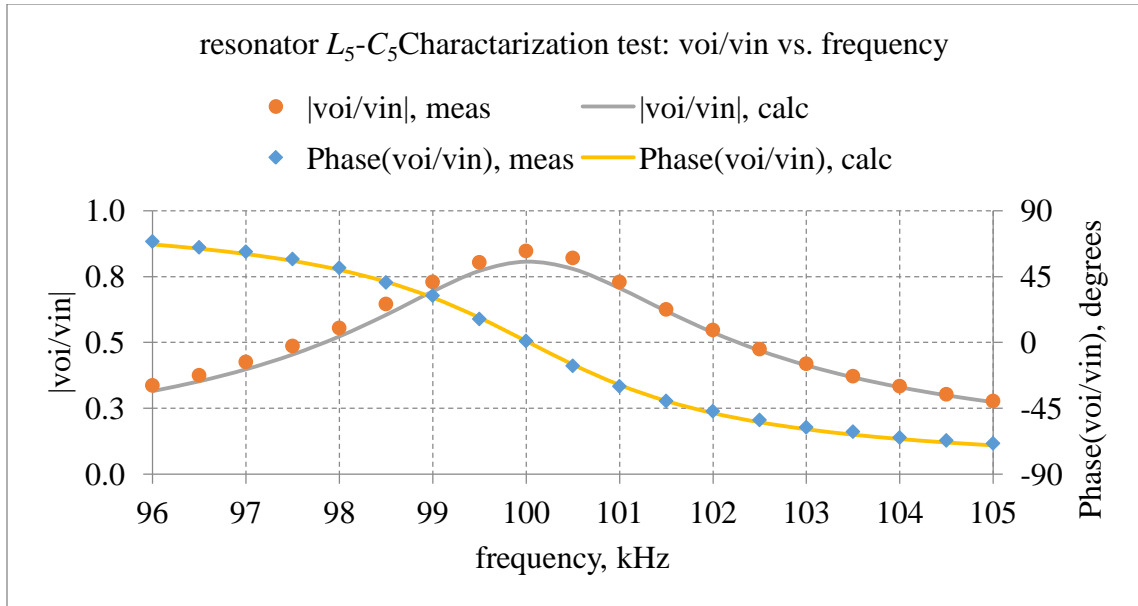
Fig. 4.12 Characterization of L_5-C_5 resonator Values of L_5=55.67 μH, C_5=45.469 nF, R_{ESR5}=0.235Ω provided the best fit of measured and calculated values

Measured parameters of the resonators of the five-resonator system are summarized in Table 4.2 below:

Table 4.2 Measured parameters *L*, *ESR*, *C*, and *f*r of resonators of five-resonator network

Resonator	*L*, μH	*C*, nF	*f*r, kHz	*ESR*, Ω
1	67.308	256.22	38.32	0.566
2	1040.18	2.4381	99.90	3.663
3	1044.99	2.4189	100.10	3.846
4	53.17	47.409	100.24	0.11
5	55.67	45.469	100.03	0.235

Using the measured parameter for *L*, *C*, f_r, and *ESR*, flux-coupling coefficient (*k*) between the pair of coils was measured using the procedure as described in Section 3.2.4; measured values of coupling coefficient are as shown in Table 4.3 below.

Table 4.3 Measured flux-coupling coefficient between pairs of resonator coils for the five-resonant network.

Resonator	1	2	3	4
L_1				
L_2	0.2448			
L_3	0.0167	0.0334		
L_4	0.0037	0.0068	0.0943	
L_5	0.0044	0.0071	0.0993	0.0294

4.4.3   Comparison of experimental and simulated results

Tests were performed to validate the simulated design of the five-coil system as discussed above. Resonator coils were planar and were arranged in parallel planes. The configuration is diagrammed in Fig. 4.7 below.

The transmitter resonator (resonator 1) was energized with a 13.5Vpp square wave at 100kHz. An Agilent 33120A arbitrary waveform generator provided the controlling waveform to the driver circuit. The driver circuit had an output resistance on the order of 0.1Ω. The receiver resonators were terminated with different combinations of load resistances; various load resistances could be obtained by placing various numbers of 50Ω non-inductive thick-film resistors in parallel. Fourier decomposition was applied to the waveforms of the driving voltage and current in resonator L_1 acquired from a digital oscilloscope. Tables below show the simulated and experimental data of the five-resonator system for the various combinations of load resistances on each of the receivers.

Tables 4.4 through Table 4.6 below show the simulated and experimental currents in resonators 1, resonator 4, and resonator 5 for various combinations of R_{L4} and R_{L5}.

Table 4.4 Simulated and experimental currents in resonator 1

vs. load resistances R_{L4} and R_{L5}

R_{L4}, Ω	R_{L5}, Ω	I_1, A (sim)	I_1, A (exp)	Φ_1, ° (exp)	Φ_1, ° (exp)
10	∞	0.081	0.088	-23.4	-25.8
∞	16.7	0.101	0.090	-25.79	-24
12.5	12.5	0.058	0.058	-17.89	-35.9
12.5	25	0.068	0.071	-19.84	-29.2
10	16.7	0.058	0.061	-18.1	-34.7
10	12.5	0.054	0.057	-17.59	-37.6

Table 4.5 Simulated and experimental current in resonator 4

vs. load resistances R_{L4} and R_{L5}

R_{L4}, Ω	R_{L5}, Ω	I_4, A (sim)	I_4, A (exp)	Φ_4, ° (exp)	Φ_4, ° (exp)
10	∞	0.176	0.171	73.67	89.1
∞	16.7	-	-	-	-
12.5	12.5	0.092	0.08	77.7	91.2
12.5	25	0.114	0.107	76.17	88.7
10	16.7	0.116	0.1043	78.68	89.5
10	12.5	0.106	0.0911	79.1	91.7

Table 4.6 Simulated and experimental current in resonator 5

vs. load resistances R_{L4} and R_{L5}

R_{L4}, Ω	R_{L5}, Ω	I_5, A (sim)	I_5, A (exp)	Φ_5, ° (exp)	Φ_5, ° (exp)
10	∞	-	-	-	-
∞	16.7	0.147	0.134	69.2	87.5
12.5	12.5	0.098	0.097	77.73	88.5
12.5	25	0.061	0.066	73.69	89.1
10	16.7	0.075	0.077	76.19	89.1
10	12.5	0.087	0.0866	77.65	88.3

Table 4.7 shows the simulated and experimental powers in the load resistors R_{L4} and R_{L5}.

Table 4.7 Simulated and experimental power in resonators 4 and 5

vs. load resistances R_{L4} and R_{L5}

R_{L4}, Ω	R_{L5}, Ω	P_4, W (sim)	P_4, W (exp)	P_5, W (sim)	P_5, W (exp)
10	∞	0.309	0.292	-	-
∞	16.7	-	-	0.362	0.300
12.5	12.5	0.105	0.079	0.12	0.118
12.5	25	0.162	0.143	0.094	0.108
10	16.7	0.135	0.108	0.094	0.099
10	12.5	0.112	0.089	0.099	0.098

Table 4.8 shows simulated and experimental power input to resonator 1 and simulated and experimental efficiencies (η).

Table 4.8 Simulated and experimental power in resonator 1 and efficiency
vs. load resistances R_{L4} and R_{L5}

R_{L4}, Ω	R_{L5}, Ω	P_1 , W (sim)	P_1, W (exp)	η , % (sim)	η , % (exp)
10	∞	0.452	0.452	68.3	64.6
∞	16.7	0.554	0.458	65.3	65.5
12.5	12.5	0.333	0.278	67.8	71
12.5	25	0.361	0.372	68.8	69.6
10	16.7	0.336	0.299	68.2	69.8
10	12.5	0.314	0.272	67.2	66.5

Experimental results are in good accordance with simulation results

4.5 Design of a WPT system with multiple resonators with two transmitters and two receivers:

After design and validation of a WPT system with two receivers, the design of a multiple resonators system with two transmitters and two receivers was undertaken. The system contains six resonators with two transmitters, two passive resonators, and two receivers.

4.5.1 System and circuit topology

The proposed mid-range multiple resonator WPT system with multiple resonators employs six resonators as in Fig. 4.13. The topology shown in Fig. 4.13 includes of six inductors: transmitting resonators L_6 and L_7; passive/self-resonator L_2; passive/self-resonator L_3; and receiver (load) resonators L_4 and L_5. Six capacitors C_2–C_7 and two load

resistances R_{L4} and R_{L5} composed of non-inductive resistors complete the system. The system is energized by a common square-wave source V_{sq} (as in Fig. 4.14) for two transmitters. Sinusoidal, steady-state analysis by means of the phasor transform may be applied to the circuit of Fig. 4.13 by decomposing the square-wave source V_{sq} into its harmonic components. For this type of analysis, V_{sq} is replaced by sinusoidal source v_s at the appropriate fundamental or harmonic frequency. In practice, the WPT network is designed such that the fundamental frequency of the square-wave source is the only constituent of the square wave that delivers significant power [36]. The output resistance of the driving square-wave source V_{sq} is R_s. Losses in each of the five loops are modeled by including equivalent series resistance (*ESR*) elements R_2–R_7. It is assumed that all six resonators are coupled through mutual inductances M_{67}, M_{62}, M_{63}, M_{64}, M_{65}, M_{72}, M_{73}, M_{74}, M_{75}, M_{23}, $M_{24,}$ $M_{25,}$ $M_{34,}$ M_{35} and M_{45}. The principal mutual inductances representing the direct path for power transfer are M_{62}, M_{72}, $M_{23,}$ $M_{34,}$ and M_{35}.
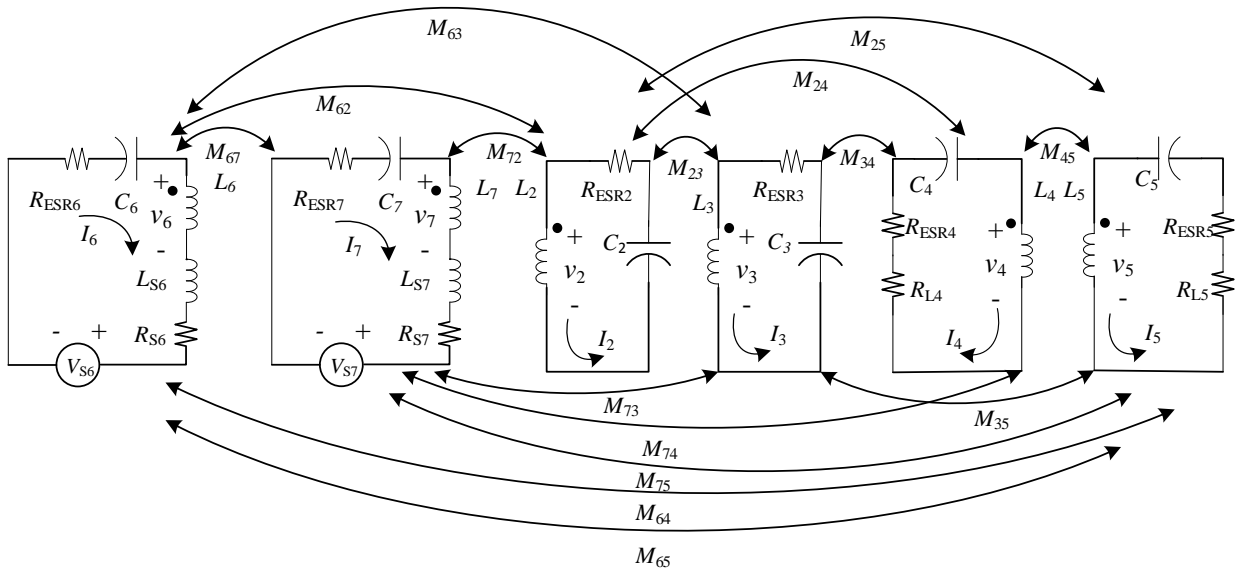
Fig. 4.13 Schematic of six-resonator WPT system
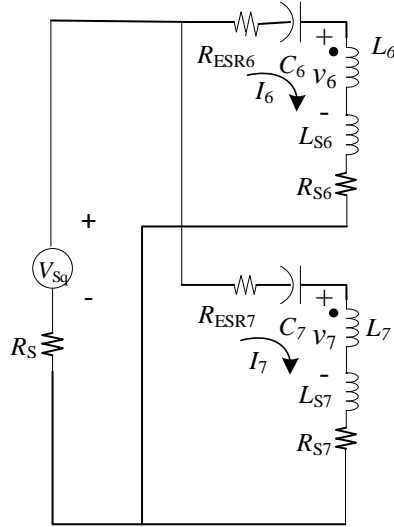
Fig. 4.14 Schematic of excitation of L_6 and L_7

4.5.2 Design of a WPT system with six resonators

The six-resonator WPT system was created by modification of the five-resonator system. This was done by replacing transmitter resonator L_1-C_1 with two transmitter resonators L_6-C_6 and L_7-C_7. L_6 and L_7 were designed identically to coils L_4 and L_5 in the five-resonator system. Separation between resonators in this design is as in Fig. 4.15.
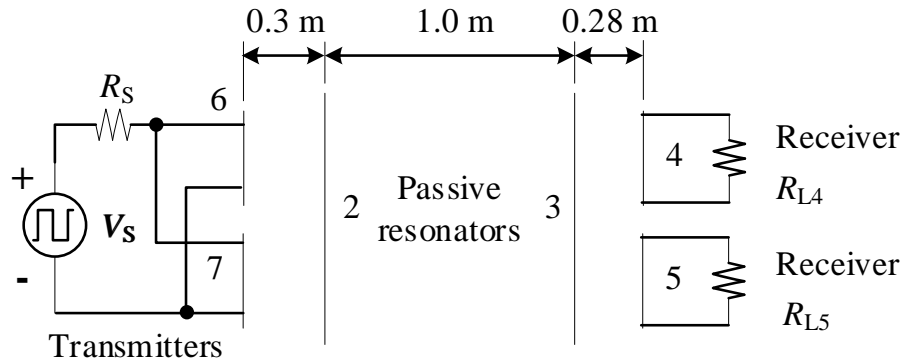
Fig. 4.15 Diagram of inductor arrangement of the six-inductor network with two receivers (loads) and two transmitters (sources), Numbers indicate resonator numbers.

Magnetic vector potential methods were then applied to compute values for flux-coupling coefficients (k) between each pair of resonator inductors for D_{23} =1m. Flux-coupling coefficients among L_2–L_5 will be unchanged because the orientations of these

coils have not changed. Table 4.9 below gives the flux-coupling coefficients related to L_6 and L_7.

Table 4.9 Flux coupling-coefficients related to resonators L_6 and L_7

Resonator	2	3	4	5	6
6	0.099699	0.007988	0.001978	0.001360	0.031502
7	0.099699	0.007988	0.001360	0.001978	

Symmetric construction of the system leads to the expectation that the coupling coefficients of coils L_6 and L_7 with L_2 will be equal; a similar argument holds for L_3.

Capacitors C_2, C_3, C_4 and C_5 were chosen to resonate with L_2, L_3, L_4 and L_5, respectively at the operating frequency of 100.0kHz; their calculated values are $C_2=C_3=2.367$nF and $C_4=C_5=45.469$nF. Capacitors C_6 and C_7 were chosen to be rather large to ensure the input impedance of the WPT network would always retain a net inductive reactance as discussed in Section 3.1.2. Both C_6 and C_7 were 300nF. The *rms* value of the fundamental component of the square wave driving the network was set to 13.50V (corresponding to a 30Vpp square wave) and the output resistance of the square-wave drive was fixed at 0.3Ω; both values are reasonable for the application. The *ESRs* were calculated (assuming Q of 200 at 100 kHz) as $R_6 = R_7 = 0.175\Omega$, $R_2 = R_3 = 3.361\Omega$, and $R_4 = R_5 = 0.175\Omega$.

4.6 Empirical design of WPT with six resonators:

4.6.1 Fabrication of load resonators for the six-resonator system

To validate the model of WPT system with six resonators as discussed in Section 4.5.2 experimentally, resonators L_6 and L_7 need to be fabricated which was done by fixing acrylic coil support and spacers on peg board as discussed in design of WPT system with five resonator. Fig. 4.16 below shows the fabricated resonators for L_6 and L_7 which are arranged side by side so that their mutual inductance is minimized, on a peg board that occupied same size for load coil in chapter 3's empirical design. These new

coils occupy the same space as the transmitter coil L1 in four- and five- coil WPT systems described in Section 3.2.1 and Section 4.4.1
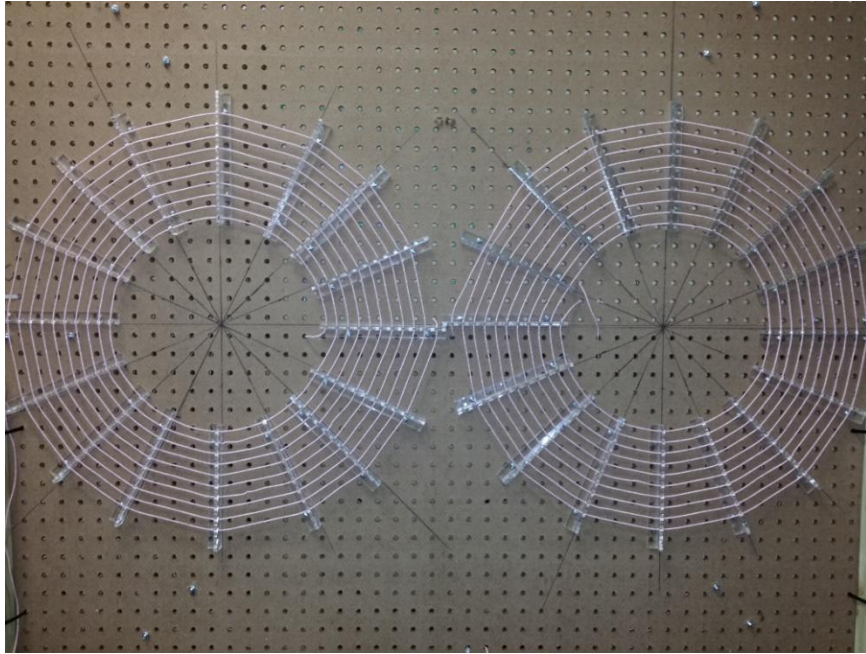
Fig. 4.16 Fabricated resonators L_7 (left) and L_6 (right)

After installing capacitors in series with transmitter resonators L_6 and L_7, they were excited with a common square wave source

4.6.2   Measurement of resonator parameters

Characterization tests (to measure parameters of resonators) of resonator were performed on all resonators. Measurements of the resonator parameters followed same procedure as discussed in Section 3.2.3. Figures, Fig. 4.17 through Fig. 4.22 below show the plots of measured and calculated values of $\left|\frac{v_{\text{oi}}}{v_{\text{in}}}\right|$ and $\angle\left(\frac{v_{\text{oi}}}{v_{\text{in}}}\right)$ vs. frequency which were obtained in the process of characterization of resonators and resonator parameter that best fits the data.
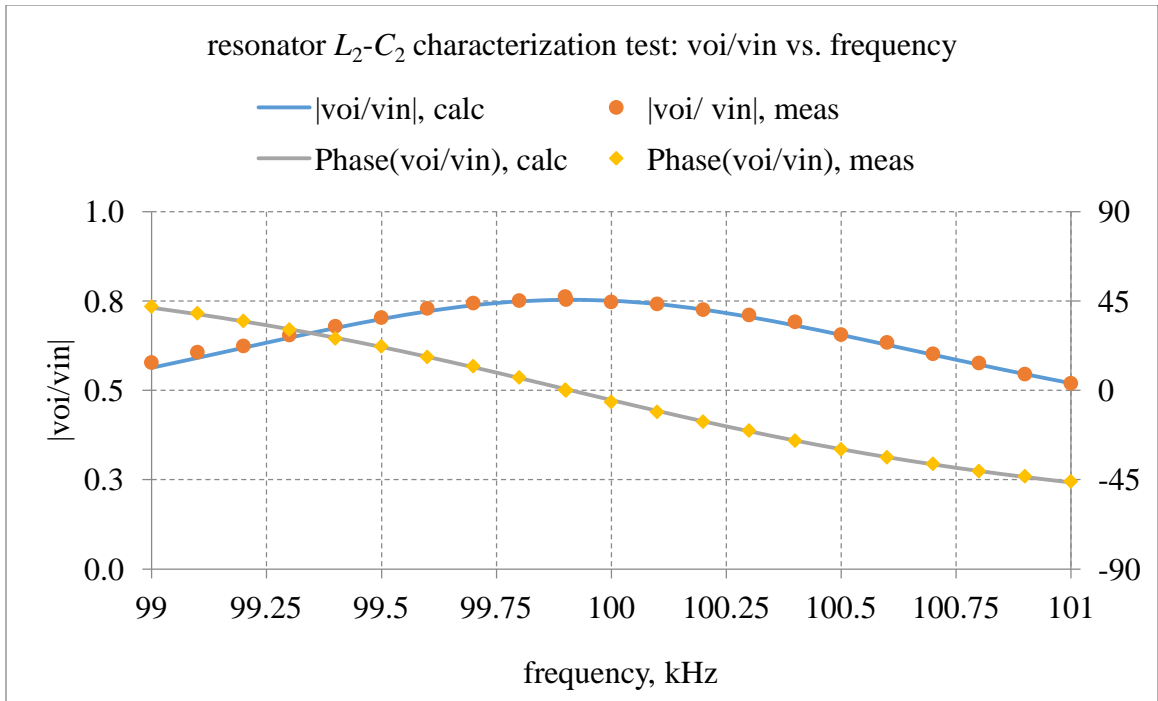
Fig. 4.17 Characterization of L_2-C_2 resonator. Values of L_2=1025.16 µH, C_2=2.475 nF, R_{ESR2}=3.256 Ω provided the best fit of measured and calculated values
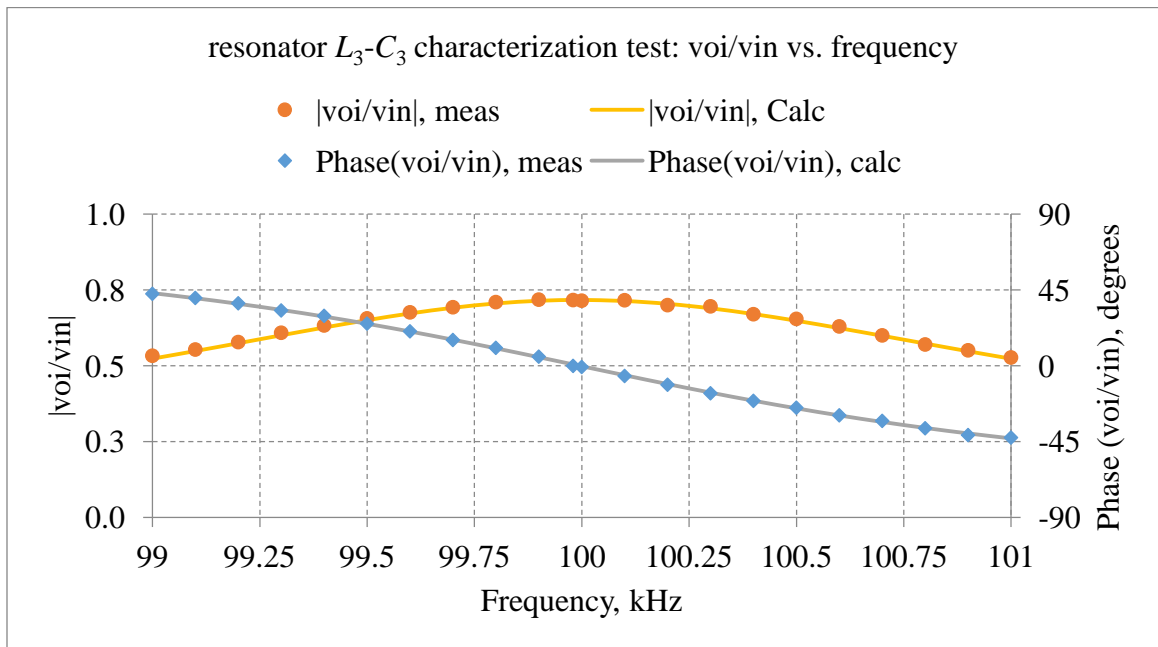
Fig. 4.18 Characterization of L_3-C_3 resonator. Values of L_3=1036.78 µH, C_3=2.443 nF, R_{ESR3}=3.932 Ω provided the best fit of measured and calculated values
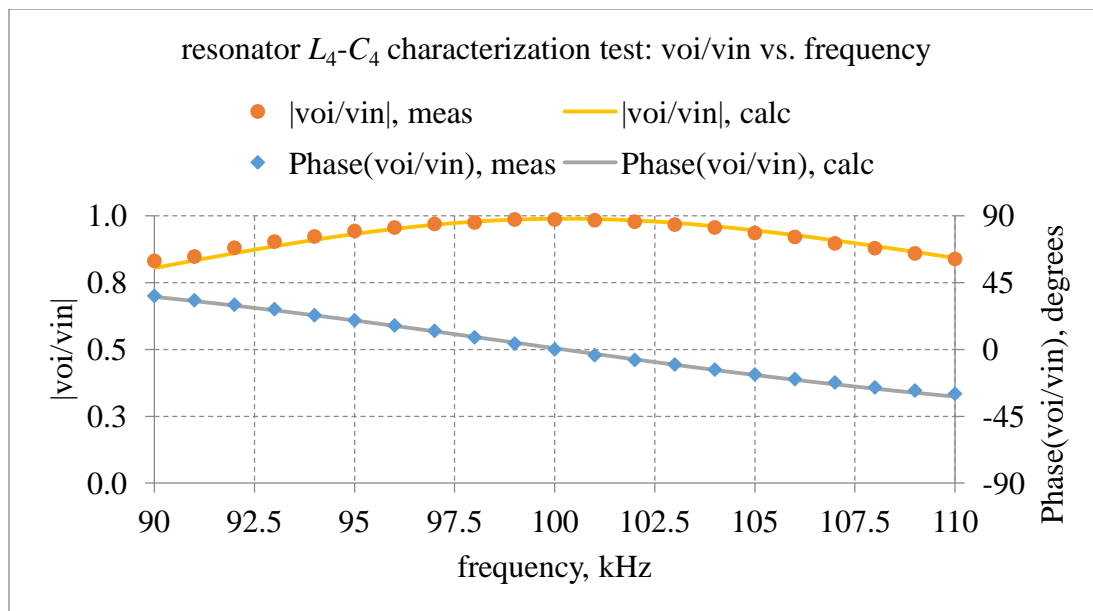
Fig. 4.19 Characterization of L_4-C_4 resonator. Values of L_4=53.17 µH, C_4=47.409 nF, R_{ESR4}=0.111Ω provided the best fit of measured and calculated values
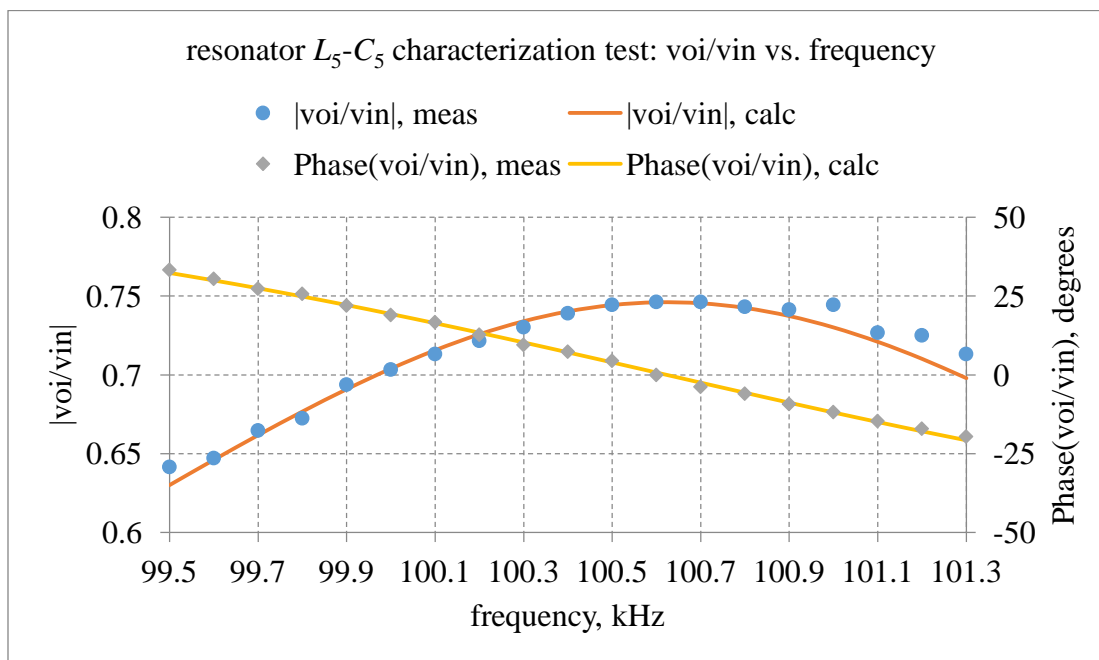
Fig. 4.20 Characterization of L_5-C_5 resonator. Values of L_5=59.83 µH, C_5=41.807 nF, R_{ESR5}=0.340 Ω provided the best fit of measured and calculated values
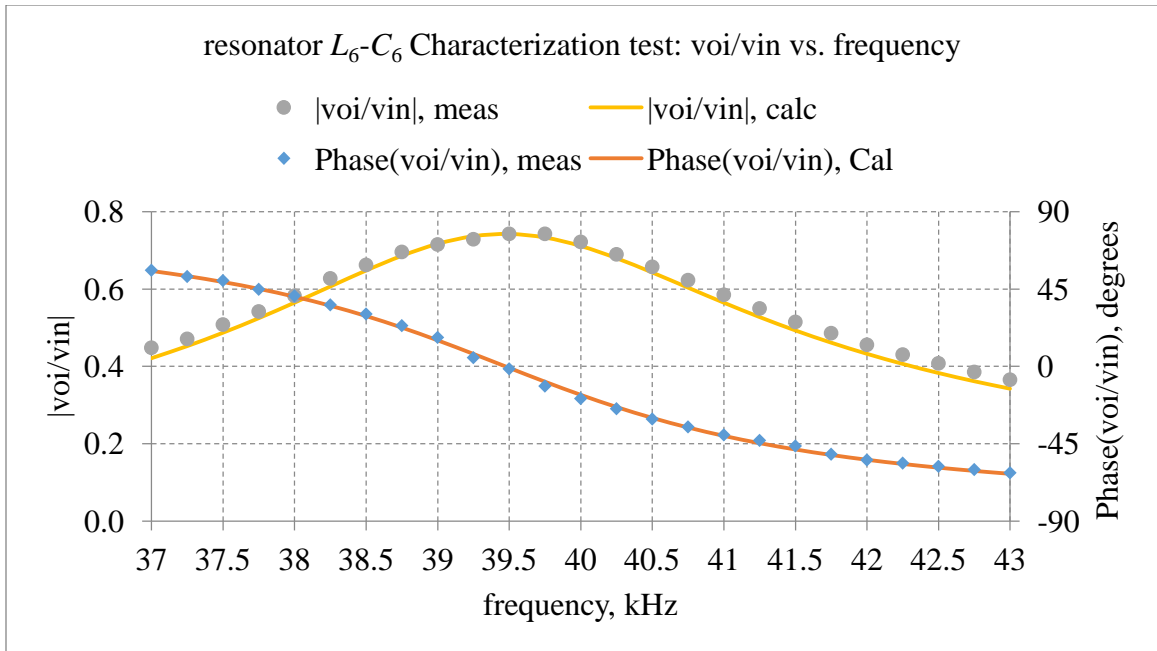
Fig. 4.21 Characterization of L_6-C_6 resonator. Values of L_6=59.85 μH, C_6=271.66 nF, R_{ESR6}=0.340 Ω provided the best fit of measured and calculated values
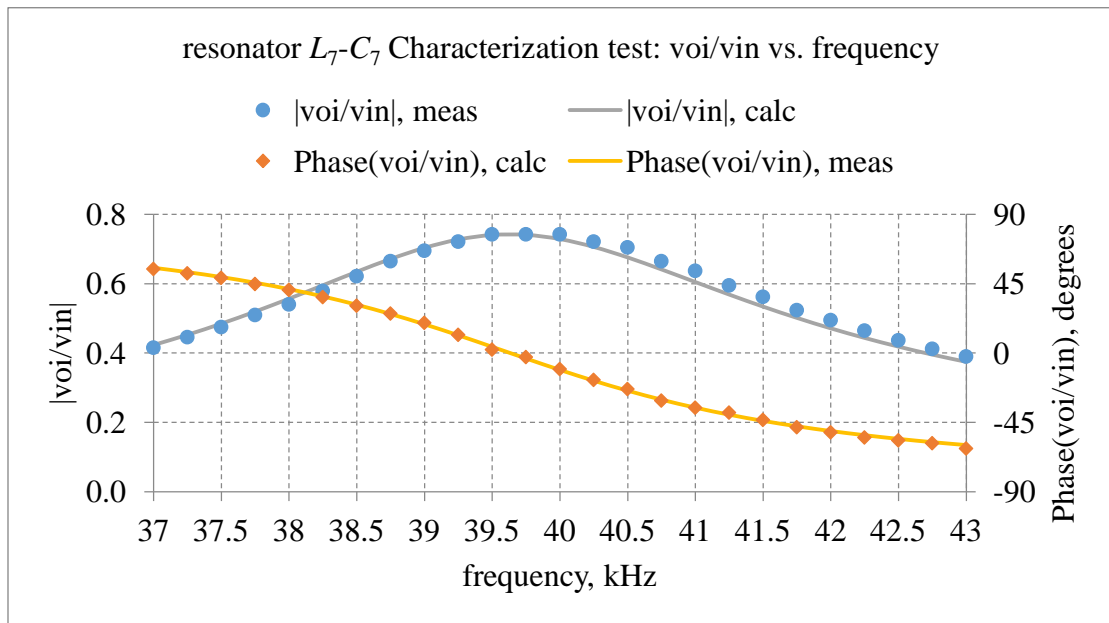
Fig. 4.22 Characterization of L_7-C_7 resonator. Values of L_7=55.64 μH, C_7=289.82 nF, R_{ESR7}=0.340 Ω provided the best fit of measured and calculated values

Measured parameters of the resonators of the six-resonator system are summarized in Table 4.10 below:

Table 4.10 Measured inductance, capacitance, ESR, and resonant frequency of the resonators of the six-resonator WPT network.

Resonator	L, μH	C, nF	f_r, kHz	R_{ESR}, Ω
L_2	1025.16	2.475	99.91	3.256
L_3	1036.78	2.443	99.99	3.932
L_4	53.17	47.409	100.2	0.111
L_5	59.83	41.807	100.62	0.340
L_6	59.85	271.66	39.47	0.340
L_7	55.64	289.82	39.47	0.340

Using the measured parameters for L, C, f_r, and *ESR*, flux-coupling coefficients (k) between the pairs of coils were measured using the procedure described in Section 3.2.4; measured values of coupling coefficients are as shown in Table 4.11 below. Gray blocks in Table 4.11 indicate repeated values of flux coupling coefficients.

Table 4.11 Measured flux-coupling coefficients between pair of resonator inductor for six-resonator network

Resonator	2	3	4	5	6
3	0.0338				
4	0.0068	0.0946			
5	0.0073	0.1047	0.0294		
6	0.0979	0.0077	0.0018	0.0014	
7	0.0836	0.0062	0.0011	0.0020	0.0236

4.6.3   Comparison of measured and simulated results for six-resonator network

Tests were performed to validate the design of the six resonator system. Resonator coils were planar and were arranged in parallel planes. The configuration is diagrammed in Fig 4.21 below.

The transmitter resonators (resonator 6 and resonator 7) were energized with a 30Vpp square wave at 100 kHz. An Agilent 33120A arbitrary waveform generator provided the controlling waveform to the driver circuit. The driver circuit had an output resistance on the order of 0.1Ω. The receiver resonators were terminated with different combinations of load resistances; various load resistances could be obtained by placing numbers of 50Ω non-inductive thick-film resistors in parallel. Fourier decomposition was applied to the waveforms of the driving point voltage and current in L_6 and L_7 acquired from a digital oscilloscope. Tables below show the simulated and experimental data on the system with six resonators for various combinations of load resistances on each of receivers.

Tables 4.12 through Table 4.15 below show the simulated and experimental currents in resonator 6, resonator 7, resonator 4, and resonator 5 for various combinations of load resistances R_{L4} and R_{L5}.

Table 4.12 Simulated and experimental current in resonator 6

vs. load resistances R_{L4} and R_{L5}

R_{L4}, Ω	R_{L5}, Ω	I_6, A (sim)	I_6, A (exp)	Φ_6 , ° (sim)	Φ_6 , ° (exp)
10	16.7	0.321	0.367	-46.07	-50.4
16.7	10	0.3123	0.34	-45.2	-45
12.5	12.5	0.3173	0.351	-45.5	-47.6
12.5	25	0.3522	0.418	-51.7	-53.7
25	12.5	0.3405	0.420	-50.3	-58.1

Table 4.13 Simulated and experimental current in resonator 7

vs. load resistances R_{L4} and R_{L5}

R_{L4}, Ω	R_{L5}, Ω	I_7, A (sim)	I_7, A (exp)	Φ_7 , ° (sim)	Φ_7 , ° (exp)
10	16.7	0.3484	0.316	-54.4	-53.2
16.7	10	0.3395	0.314	-54	-51.3
12.5	12.5	0.3441	0.308	-54.0	-49.9
12.5	25	0.3788	0.3424	-58.3	-58.6
25	12.5	0.3677	0.375	-57.41	-59.7

Table 4.14 Simulated and experimental current in resonator 4

vs. load resistances R_{L4} and R_{L5}

R_{L4}, Ω	R_{L5}, Ω	I_4, A (sim)	I_4, A (exp)	Φ_4 , ° (sim)	Φ_4 , ° (exp)
10	16.7	0.458	0.442	45.1	58.2
16.7	10	0.2656	0.243	43	65.2
12.5	12.5	0.3606	0.343	44.3	61.1
12.5	25	0.4215	0.406	39.7	52.6
25	12.5	0.2028	0.190	38.2	55.8

Table 4.15 Simulated and experimental current in resonator 5

vs. load resistances R_{L4} and R_{L5}

R_{L4}, Ω	R_{L5}, Ω	I_5, A (sim)	I_5, A (exp)	Φ_5 , ° (sim)	Φ_5 , ° (exp)
10	16.7	0.3191	0.335	44.7	57.8
16.7	10	0.5012	0.5127	48.5	57.3
12.5	12.5	0.4136	0.4326	46.8	57.8
12.5	25	0.2465	0.254	38.6	49.7
25	12.5	0.462	0.467	43.1	50.1

Table 4.16 shows the simulated and experimental power dissipation in load resistors R_{L4} and R_{L5} vs. load resistances R_{L4} and R_{L5}.

Table 4.16 Simulated and experimental power dissipation in load resistances R_{L4} and R_{L5}

R_{L4}, Ω	R_{L5}, Ω	P_4 , W (sim)	P_4, W (exp)	P_5, W (sim)	P_5, W (exp)
10	16.7	2.097	1.951	1.7	1.874
16.7	10	1.178	0.982	2.512	2.629
12.5	12.5	1.625	1.474	2.138	2.339
12.5	25	2.221	2.062	1.519	1.609
25	12.5	1.028	0.900	2.668	2.725

Table 4.17 shows simulated and experimental power input to resonator 6 and resonator 7 and Table 4.18 shows simulated and experimental efficiencies (η).

Table 4.17 Simulated and experimental power in resonators 6 and 7

vs. load resistances R_{L4} and R_{L5}

R_{L4}, Ω	R_{L5}, Ω	P_6, W (sim)	P_6, W (exp)	P_7, W (sim)	P_7, W (exp)
10	16.7	3.015	3.164	2.74	2.572
16.7	10	2.972	3.248	2.698	2.649
12.5	12.5	3.006	3.212	2.731	2.685
12.5	25	2.948	3.364	2.688	2.422
25	12.5	2.939	2.981	2.675	2.519

Table 4.18 Simulated and experimental efficiency vs. load resistances R_{L4} and R_{L5}

R_{L4}, Ω	R_{L5}, Ω	η, % (sim)	η, % (exp)
10	16.7	66	66.7
16.7	10	65.1	61.2
12.5	12.5	65.6	64.7
12.5	25	66.4	63.4
25	12.5	65.8	65.9

Experimental results and simulated values were largely in line, except for the measured phase of current I_4. The expected reason for the differences is due to highly sensitive nature of system to input parameters. It is found that a slight change in the value of the coupling coefficient k_{34} the difference between the experimental and simulated phases of I4 could be reduced.

4. 7 Summary

The design of WPT system with multiple resonators with loose coupling has been validated with both theoretical and experimental data and both have been found matching

and error within 5%. Tool designed using spreadsheet has also been successfully validated with theoretical and experimental data. For a WPT system with multiple resonators, case with one power source (transmitter) and two loads (receiver) and case with two power sources (transmitters) and two loads (receivers) has been successfully verified.

Chapter Five
Conclusion

5. 1 Conclusions

The primary data gathered from the experiments performed are useful in shaping the future of wireless power transfer, as it progresses toward goals of high power and high efficiency. In this thesis, design and analysis of WPT systems involving four, five, and six coils have been validated by experiment. Methodologies for measuring resonator parameters and for measuring mutual inductances are also described. The efficiency reached by the experimental model (incorporating a single source and load) described in Chapter Three reached about 70% with an air gap distance of 1m between transmitting and receiving resonators. A model for WPT networks including an arbitrary number of resonators has been proposed. An analysis tool for WPT designs including up to eight resonators at a time has been modeled. The simulated work was validated by experiment for five- and six-resonator WPT systems. The efficiency reached by the experimental five-resonator network described in Chapter Four reached about 70% with an air gap of 1m between the source and load resonators. It was also found that efficiency of system was improved with two loads acting on a system. Later, a six-resonator system with two sources and two receivers was also experimentally validated. The efficiency reached by the six resonator system was about 68% for a separation of 1m between the transmitter and receiver resonators.

5. 2 Future work

The immediate extension of this thesis could be validating the designed four-coil method under different resonator-to-resonator separations and with nonlinear (instead of resistive) loads. Work could also be undertaken for empirical validation of multiple-resonator systems with various physical configurations (e.g., arrangement of resonators in

a circle or resonators in parallel offset lines for "leapfrog" power transfer). In addition, modeling and validation with realistic loads (including nonlinear loads) could be a fruitful area of research

References

[1] http://en.wikipedia.org/wiki/Tesla_coil , accessed on March 23, 2014.

[2] http://www.tfcbooks.com/articles/witricity.htm , accessed on March 23, 2014.

[3] Marincic, A.S., "Nikola Tesla and the Wireless Transmission of Energy," *Power Apparatus and Systems, IEEE Transactions on*, vol.PAS-101, no.10, pp.4064-4068, Oct. 1982.

[4] http://www.tfcbooks.com/tesla/1898-11-17.htm , accessed on March 23, 2014.

[5] N. Tesla, "Apparatus for Transmission of Electrical Energy," U.S. Patent 649621 A, May 15, 1900.

[6] http://www.tfcbooks.com/articles/tws8b.htm , accessed on March 23, 2014.

[7] http://www.rish.kyoto-u.ac.jp/SPS/WPAppendicesStd.pdf, "Appendix A Microwave Power Transmission Activities in the World".

[8] Ick-Jae Yoon and Hao Ling (2012). Realizing Efficient Wireless Power Transfer in the Near-Field Region Using Electrically Small Antennas, Wireless Power Transfer - Principles and Engineering Explorations, Dr. Ki Young Kim (Ed.), ISBN: 978-953-307-874-8, InTech, DOI: 10.5772/28897.

[9] http://www.teslasociety.com/teslabanquet.htm , accessed on March 23, 2014.

[10] R. S. Mackay and B. Jacobson, "Endo Radiosonde," Nature, vol. 179, pp.1239-1240; June 15, 1957.

[11] Mackay, R.S., "Radio Telemetering from Within the Human Body," *Medical Electronics, IRE Transactions on*, vol.ME-6, no.2, pp.100-105, June 1959.

[12] Nagumo, J.; Uchiyama, A.; Kimoto, S.; Watanuki, T.; Hori, M.; Suma, K.; Ouchi, A.; Kumano, M.; Watanabe, H., "Echo Capsule for Medical Use (A Batteryless Endoradiosonde)," *Bio-Medical Electronics, IRE Transactions on* , vol.9, no.3, pp.195-199, July 1962.

[13] Kurs, A. Karalis, R. Moffatt, J. D. Joannopoulos, P. Fisher, and M. Soljacic, "Wireless Power Transfer via Strongly Coupled Magnetic Resonances," Science vol.317, no.5834, pp. 83-86, June 2007.

[14] http://techon.nikkeibp.co.jp/article/HONSHI/20100420/181986/z1s.jpg , accessed on March 23, 2014.

[15] http://www.wirelesspowerconsortium.com/about/ , accessed on March 23, 2014.

[16] http://www.qiwireless.com/wireless-power-consortium-extend-qi-standard-add-resonance-charging/ , accesses on March 23, 2014.

[17] http://newsroom.intel.com/docs/DOC-1119 , accessed on March 23, 2014.

[18] http://www.qualcomm.com/solutions/wireless-charging/wipower , accessed on March 23, 2014.

[19] http://www.wirelesspowerplanet.com/news/the-future-of-wireless-power/ , accessed on March 23, 2014.

[20] http://www.theengineer.co.uk/in-depth/analysis/europes-biggest-wireless-charging-trial-begins-in-london/1012047.article , accessed on March 23, 2014.

[21] http://phys.org/news/2012-01-qualcomm-haloipt-tech-wireless-evs.html , accessed on March 26, 2014.

[22] http://techon.nikkeibp.co.jp/english/NEWS_EN/20120115/203612/ , accessed on March 26, 2014.

[23] Zierhofer, C.M.; Hochmair, E.S., "Geometric approach for coupling enhancement of magnetically coupled coils," *Biomedical Engineering, IEEE Transactions on*, vol.43, no.7, pp.708-714, July 1996.

[24] Kim, Y.; Ling, H., "Investigation of coupled mode behaviour of electrically small meander antennas," *Electronics Letters*, vol.43, no.23, November 8, 2007.

[25] Imura, T.; Okabe, H.; Hori, Y., "Basic experimental study on helical antennas of wireless power transfer for Electric Vehicles by using magnetic resonant couplings," *Vehicle Power and Propulsion Conference, 2009* (VPPC '09) *IEEE*, pp.936-940, 7-10 September 2009.

[26] Teck Chuan Beh; Imura, T.; Kato, M.; Hori, Y., "Basic study of improving efficiency of wireless power transfer via magnetic resonance coupling based on impedance matching," *Industrial Electronics (ISIE), 2010 IEEE International Symposium on*, pp.2011-2016, 4-7 July 2010.

[27] Ng, D.C.; Boyd, C.; Bai, S.; Felic, G.; Halpern, M.; Skafidas, E., "High-Q flexible spiral inductive coils," *Electromagnetic Compatibility Symposium - Melbourne (EMC Melbourne), 2010*, pp.1-4, 8-10 September 2010.

[28] Taylor, J.A.; Zhen Ning Low; Casanova, J.; Jenshan Lin, "A wireless power station for laptop computers," *Radio and Wireless Symposium (RWS), 2010 IEEE* , pp.625-628, 10-14 January 2010.

[29] Jin Wook Kim; Hyeon-Chang Son; Kwan-Ho Kim; Young-Jin Park, "Efficiency Analysis of Magnetic Resonance Wireless Power Transfer With Intermediate Resonant Coil," *Antennas and Wireless Propagation Letters, IEEE* , vol.10, no., pp.389-392, 2011.

[30] Imura, T.; Hori, Y., "Maximizing Air Gap and Efficiency of Magnetic Resonant Coupling for Wireless Power Transfer Using Equivalent Circuit and Neumann Formula," *Industrial Electronics, IEEE Transactions on*, vol.58, no.10, pp.4746-4752, October 2011.

[31] Seung-Hwan Lee; Lorenz, R.D., "A design methodology for multi-kW, large air-gap, MHz frequency, wireless power transfer systems," *Energy Conversion Congress and Exposition (ECCE), 2011 IEEE*, pp.3503-3510, 17-22 September 2011.

[32] Sample, A.P.; Meyer, D.A.; Smith, J.R., "Analysis, Experimental Results, and Range Adaptation of Magnetically Coupled Resonators for Wireless Power Transfer," *Industrial Electronics, IEEE Transactions on*, vol.58, no.2, pp.544-554, February 2011.

[33] Jinwook Kim; Hyeon-Chang Son; Do-Hyeon Kim; Young-Jin Park, "Optimal design of a wireless power transfer system with multiple self-resonators for an LED TV," *Consumer Electronics, IEEE Transactions on* , vol.58, no.3, pp.775-780, August 2012.

[34] Kiani, M. and Ghovanloo, M., "The Circuit Theory Behind Coupled-Mode Magnetic Resonance-Based Wireless Power Transmission," *Circuits and Systems I: Regular Papers, IEEE Transactions on*, vol.59, no.9, pp.2065-2074, September 2012.

[35] Beams, D.M. and Annam, S.G., "Calculation of mutual inductance from magnetic vector potential for wireless power transfer applications," *System Theory (SSST), 2012 44th Southeastern Symposium on*, pp.209-213, 11-13 March 2012.

[36] Beams, D.M. and Annam, S.G., "Validation of a reflected-impedance design method for wireless power transfer applications," *Circuits and Systems (MWSCAS), 2012 IEEE 55th International Midwest Symposium on*, pp.758-761, 5-8 August 2012.

[37] Annam.S, "Four-coil Wireless Power Transfer using resonant inductive coupling", Master's Thesis, University of Texas at Tyler, 2012.

[38] Beams, D.M. and Nagoorkar, V., "Design and simulation of networks for midrange wireless power transfer," *Circuits and Systems (MWSCAS), 2013 IEEE 56th International Midwest Symposium on*, pp.509-512, 4-7 August 2013

[39] Beams, D.M. and Papasani, A., "State-variable analysis of wireless power transfer networks for linear and nonlinear loads," *Circuits and Systems (MWSCAS), 2013 IEEE 56th International Midwest Symposium on*, pp.505-508, 4-7 August 2013.

[40] RamRakhyani, A.K.; Mirabbasi, S.; Mu Chiao, "Design and Optimization of Resonance-Based Efficient Wireless Power Delivery Systems for Biomedical Implants," *Biomedical Circuits and Systems, IEEE Transactions on*, vol.5, no.1, pp.48-63, February 2011.

[41] C.K. Lee, W.X. Zhong and S.Y.R. Hui. "Recent Progress in Mid-Range Wireless Power Transfer" IEEE Energy Conversion Congress and Exposition (ECCE), pp.3819-3824, 15-20 September, 2012.

[42] Sanghoon Cheon; Yong-Hae Kim; Kang, Seung-Youl; Myung-Lae Lee; Jong-Moo Lee; Zyung, Taehyoung, "Circuit-Model-Based Analysis of a Wireless Energy-Transfer System via Coupled Magnetic Resonances," *Industrial Electronics, IEEE Transactions on* , vol.58, no.7, pp.2906-2914, July 2011.

[43] Beams, D.M.; Annam, S.G., "Failure mechanisms in MOSFET square-wave drivers for wireless power transfer applications," *System Theory (SSST), 2013 45th Southeastern Symposium on*, pp.1-5, 11-11 March 2013.

[44] Kurs, Andre; Moffatt, Robert; Soljacic, Marin, "Simultaneous mid-range power transfer to multiple devices," *Applied Physics Letters*, vol.96, no.4, pp.044102-044102-3, January 2010.

[45] Jin-Wook Kim; Hyeon-Chang Son; Do-Hyun Kim; Kwan-Ho Kim; Young-Jin Park, "Analysis of wireless energy transfer to multiple devices using CMT," *Microwave Conference Proceedings (APMC), 2010 Asia-Pacific* , pp.2149-2152, 7-10 December 2010.

[46] Bong wan Jun, B.S, "An Investigation on Transmitter and Receiver Diversity for Wireless Power Transfer ", Master's Thesis, The University of Texas at Austin, 2011.

[47] Jinwook Kim; Hyeon-Chang Son; Do-Hyeon Kim; Jong-Ryul Yang; Kwan-Ho Kim; Ki-Min Lee; Young-Jin Park, "Wireless power transfer for free positioning using compact planar multiple self-resonators," *Microwave Workshop Series on Innovative Wireless Power Transmission: Technologies, Systems, and Applications (IMWS), 2012 IEEE MTT-S International* , pp.127-130, 10-11 May 2012.

[48] Dukju Ahn; Songcheol Hong, "Effect of Coupling between Multiple Transmitters or Multiple Receivers on Wireless Power Transfer," *Industrial Electronics, IEEE Transactions on*, vol.60, no.7, pp.2602-2613, July 2013.

[49] Seungyong Shin; Jaegue Shin; Boyune Song; Seokhwan Lee; Yangsu Kim; Guho Jung; Seongjeub Jeon, "Wireless power transfer system for high power application and a method of segmentation," *Wireless Power Transfer (WPT), 2013 IEEE* , pp.76-78, 15-16 May 2013.

[50] Lee, K.; Pantic, Z.; Lukic, S.M., "Reflexive Field Containment in Dynamic Inductive Power Transfer Systems," *Power Electronics, IEEE Transactions on*, vol.29, no.9, pp.4592-4602, September 2014.